



# POLITECNICO MILANO 1863

School of Industrial and Information Engineering

Master of Science in Space Engineering

Course: Space Systems Engineering and Operations

Professor: Michèle Roberta Lavagna



## *JASON-2/OSTM* *Ocean Surface Topography Mission*

A.Y. 2023/2024

### Final Delivery Team 3

Camilla Airoldi	10709904
Didier Bontemps	10911352
Leo De Luca	10694949
Elena De Marco	10753159
Gianluca Perusini	10987083
Viola Poverini	11013026

July 6, 2024

# Contents

<b>Homework 1: Mission Overview</b>	<b>1</b>
<b>1 Introduction</b>	<b>2</b>
<b>2 High Level Goals</b>	<b>2</b>
<b>3 Mission Drivers</b>	<b>2</b>
<b>4 Functional Analysis</b>	<b>3</b>
<b>5 Mission Phases and Correlation to Functionalities</b>	<b>3</b>
<b>6 Concept of Operations</b>	<b>4</b>
<b>7 Goal-P/Ls Functions Correlation</b>	<b>5</b>
7.1 Main Payloads Overview . . . . .	5
7.2 Mission Goals-P/Ls Functions Correlation . . . . .	6
7.3 Additional Payloads . . . . .	6
7.4 P/Ls - ConOps/Phases Correlation . . . . .	6
<b>8 Mission Analysis Understanding</b>	<b>7</b>
8.1 Trajectory Design . . . . .	7
8.2 Functionalities-Phases Correlation to Trajectory Design . . . . .	8
<b>Homework 2: Mission Analysis &amp; Propulsion Subsystem</b>	<b>9</b>
<b>1 Homework 2.1</b>	<b>10</b>
1.1 Mission trajectory design . . . . .	10
1.2 Reverse engineering of $\Delta V$ budget . . . . .	11
1.3 $\Delta V$ budget breakdown and margins . . . . .	11
<b>2 Homework 2.2</b>	<b>12</b>
2.1 Mission propulsion architecture . . . . .	12
2.2 Primary and secondary propulsion . . . . .	13
2.3 Justification of propulsion type and architecture . . . . .	13
2.4 Reverse sizing . . . . .	13
2.4.1 Propellant selection and masses . . . . .	13
2.4.2 Tank Sizing . . . . .	14
2.4.3 Pressurant selection and masses . . . . .	15
2.4.4 Feeding strategy selection and sizing . . . . .	15
2.4.5 Number and positioning of thrusters . . . . .	16
2.4.6 Positioning of tank and lines in the configuration . . . . .	16
2.5 Budget . . . . .	16
<b>Homework 3: Tracking Telemetry &amp; Telecommand Subsystem</b>	<b>17</b>
<b>1 TTMTTC Subsystem</b>	<b>18</b>
1.1 Tracking . . . . .	18
1.2 Telemetry and Telecommand . . . . .	18
1.3 Ground Segment . . . . .	19
<b>2 TTMTTC operations</b>	<b>19</b>
2.1 Phases . . . . .	19
2.2 Modes . . . . .	19
2.3 TTMTTC Data Volume . . . . .	19

<b>3 Reverse sizing</b>	<b>20</b>
3.1 Antenna Selection . . . . .	20
3.2 Frequency Selection, Datarate, and Band . . . . .	20
3.3 Losses . . . . .	20
3.4 Signal Manipulation . . . . .	21
Encoding . . . . .	21
Modulation . . . . .	21
Amplification . . . . .	21
3.5 Link Budget . . . . .	21
3.6 Ground Station Selection . . . . .	22
3.7 Antenna Positioning . . . . .	22
3.8 TTMTTC Budget . . . . .	22
<b>Homework 4: Attitude Determination &amp; Control Subsystem</b>	<b>22</b>
<b>1 AOCS Architecture</b>	<b>24</b>
1.1 Attitude Determination . . . . .	24
1.1.1 Sensors . . . . .	24
1.1.2 Attitude Determination Algorithm . . . . .	24
1.2 Attitude and Orbit Control . . . . .	25
1.2.1 Actuators . . . . .	25
1.2.2 Attitude Control Algorithm . . . . .	25
<b>2 Operational Modes</b>	<b>26</b>
<b>3 AOCS Pointing Budget</b>	<b>27</b>
<b>4 Reverse Sizing</b>	<b>27</b>
4.1 Attitude Sensor Suite Selection . . . . .	27
4.2 Attitude Actuator Suite Selection . . . . .	27
4.3 Disturbances Effects . . . . .	28
4.3.1 Perturbing Torques . . . . .	29
4.4 Attitude Actuators Sizing . . . . .	29
4.4.1 Desaturation . . . . .	29
4.4.2 Slew Manoeuvres . . . . .	29
4.5 Fuel Mass Sizing . . . . .	30
4.6 Positioning of Sensors and Actuators . . . . .	30
4.7 Subsystem Budgets . . . . .	30
<b>Homework 5: Thermal Control Subsystem</b>	<b>30</b>
<b>1 TCS Architecture</b>	<b>32</b>
1.1 Passive Control . . . . .	32
1.2 Active Control . . . . .	32
1.2.1 ATC Algorithm . . . . .	32
<b>2 Thermal control description and rationale</b>	<b>33</b>
<b>3 External and Internal heat fluxes along the phases</b>	<b>33</b>
3.1 External flux . . . . .	33
3.2 Internal fluxes . . . . .	34
<b>4 Requested temperature intervals</b>	<b>34</b>
<b>5 TCS Sizing</b>	<b>34</b>
5.1 Environment modeling . . . . .	34
5.1.1 Material selection and coating . . . . .	35
5.2 Hot case sizing . . . . .	35
5.2.1 Radiator sizing . . . . .	36
5.3 Cold case . . . . .	36
5.3.1 Heater sizing . . . . .	36
5.4 Specifically controlled units . . . . .	36
5.5 Adopted control strategy . . . . .	37
5.6 Position and pointing . . . . .	37

5.7 Subsystem budget . . . . .	37
<b>Homework 6: Electric Power Subsystem</b>	<b>37</b>
<b>1 EPS Architecture</b>	<b>39</b>
1.1 Primary Power Source: Solar Arrays . . . . .	39
1.2 Energy Storage: Secondary Battery . . . . .	39
1.3 Power Control and Distribution . . . . .	39
<b>2 EPS architecture according to Phases/Modes</b>	<b>40</b>
2.1 Power requirements per modes . . . . .	40
<b>3 Operational profiles and available sources</b>	<b>40</b>
3.1 Payload power profile in early orbit phase . . . . .	41
<b>4 EPS Sizing</b>	<b>42</b>
4.1 Power Budget per mode . . . . .	42
4.2 Primary source selection and sizing . . . . .	42
4.3 Secondary source selection and sizing . . . . .	43
4.4 Primary source regulation adopted strategy . . . . .	44
4.5 Bus regulation adopted strategy . . . . .	44
4.6 Positioning of components and pointing requirements . . . . .	44
4.7 Subsystem budget . . . . .	44
<b>Homework 7: Configuration &amp; On-Board Data Handling</b>	<b>44</b>
<b>1 Configuration</b>	<b>46</b>
1.1 Vehicle shape and appendages distribution . . . . .	46
1.2 Launch configuration . . . . .	46
1.3 External Configuration . . . . .	47
1.3.1 Propulsion System . . . . .	47
1.3.2 AOCS . . . . .	47
1.3.3 Thermal . . . . .	47
1.3.4 EPS . . . . .	47
1.3.5 TTMTTC . . . . .	47
1.3.6 Payload . . . . .	47
1.4 Internal configuration . . . . .	48
1.4.1 Propulsion . . . . .	48
1.4.2 AOCS . . . . .	48
1.4.3 Thermal . . . . .	48
1.4.4 EPS . . . . .	48
1.4.5 OBDH . . . . .	48
1.4.6 Payload . . . . .	48
<b>2 OBDH Architecture</b>	<b>49</b>
2.1 Payload data . . . . .	49
2.2 OBDH processor . . . . .	50
2.3 OBDH adopted bus . . . . .	50
<b>3 OBDH sizing</b>	<b>51</b>
3.1 On Board Computer and Memory Sizing . . . . .	51

## Nomenclature

<i>ADCS</i>	Attitude Determination Control Subsystem
<i>AKE</i>	Absolute Knowledge Error
<i>APE</i>	Absolute Pointing Error
<i>ATC</i>	Active Thermal Control
<i>AU</i>	Astronomical Unit
<i>B</i>	Blow-down ratio
<i>BER</i>	Bit Error Rate
<i>BOL</i>	Beginning Of Life
<i>BPSK</i>	Binary Phase Shift Keying
<i>CNES</i>	Centre National d'Etudes Spatiales
<i>CoM</i>	Centre of Mass
<i>ConOps</i>	Concept of Operations
<i>DET</i>	Direct Energy Transfer
<i>DoD</i>	Depth of Discharge
<i>DOF</i>	Degree Of Freedom
<i>DS</i>	Deep Space
<i>DSN</i>	Deep Space Network
<i>ECSS</i>	European Cooperation for Space Standardization
<i>EOL</i>	End Of Life
<i>EPDM</i>	Ethylene Propylene Diene Monomer
<i>EPS</i>	Electrical Power Subsystem
<i>ESA</i>	European Space Agency
<i>EUMETSAT</i>	European Organisation for the Exploitation of Meteorological Satellites
<i>GDR</i>	Geophysical Data Record
<i>GG</i>	Gravity Gradient
<i>GPS</i>	Global Positioning System
<i>GS</i>	Ground Station
<i>IGDR</i>	Interim Geophysical Data Record
<i>iLRO</i>	interleaved Long Repeat Orbit
<i>LEO</i>	Low Earth Orbit
<i>LEOP</i>	Low Earth Orbit Parking
<i>LRA</i>	Laser Retroreflector Array
<i>MLI</i>	Multi Layer Insulation
<i>MPS</i>	Monopropellant Propulsion System
<i>MR</i>	Mass Ratio
<i>MTB</i>	Magnetic Torquer Bar
<i>NASA</i>	National Aeronautics and Space Administration

<i>NOAA</i>	National Oceanic and Atmospheric Administration
<i>OBC</i>	On-Board Computer
<i>OBDH</i>	On-Board Data Handling
<i>OGDR</i>	Operational Geophysical Data Record
<i>OSK</i>	Orbit Station Keeping
<i>OSTM</i>	Ocean Surface Topography Mission
<i>P/L</i>	Payload
<i>PAF</i>	Payload Attach Fitting
<i>PEPT</i>	Positive Expulsion Propellant Tank
<i>POD</i>	Precision Orbit Determination
<i>PPT</i>	Peak Power Tracking
<i>PROTEUS</i>	Plateforme Reconfigurable pour l'Observation, les Télécommunications et les Usages Scientifiques
<i>PV</i>	Photovoltaic
<i>QPSK</i>	Quadratic Phase Shift Keying
<i>RAM</i>	Random Access Memory
<i>RW</i>	Reaction wheels
<i>S/C</i>	Spacecraft
<i>SAA</i>	South Atlantic Anomaly
<i>SHM</i>	Safe Hold Mode
<i>SLR</i>	Satellite Laser Ranging
<i>SMA RV</i>	Semi Major Axis Rendez-vous
<i>SNR</i>	Signal to Noise Ratio
<i>SRP</i>	Solar Radiation Pressure
<i>SSA</i>	Solid State Amplifier
<i>SSM</i>	Second Surface Mirror
<i>STR</i>	Star Tracker
<i>T/P</i>	TOPEX/Poseidon
<i>TCS</i>	Thermal Control Subsystem
<i>TOF</i>	Time Of Flight
<i>TOPEX</i>	Topography Experiment
<i>TP</i>	Throughput
<i>TTMTC</i>	Tracking Telemetry and Telecommand

# **Homework 1**

## **Mission Overview**

# 1 Introduction

The ocean is the single most significant influence on Earth's climate and weather [68]. The Ocean Surface Topography Jason-2 mission, a collaborative effort by NASA, CNES, NOAA and EUMETSAT, has significantly advanced our understanding of this great reservoir with measurements of global sea-level change, tide models and ocean circulation.

Launched in June 20, 2008 by a Delta II 7320 rocket, Jason-2 has followed the footsteps of the previous Poseidon/TOPEX and Jason-1 missions and was able to successfully extend the continuous record of observations until its final disposal in October 2019.

In this report, an initial reverse engineering process is presented by identifying and understanding the mission objectives, structure, activities and trajectory design.

## 2 High Level Goals

The high level goals that set the baseline to the mission are the following:

1. Extend the time series of ocean surface topography measurements beyond TOPEX/Poseidon and Jason-1 covering a continuous period of two decades overall[68];
2. Acquire near-real time high-precision altimetric measurements to be integrated into ocean forecasting models;
3. Enhance the accuracy of measurements of global sea level variations and monitor its relation to global climate change;
4. Determine the long-term variability of ocean circulation by combining data records from OSTM/Jason-2 with those of TOPEX/Poseidon and Jason-1[67];
5. Improve open ocean tide and weather models.

Subsection 7.2 shows how these scientific objectives have been achieved through the use of one or more P/Ls.

## 3 Mission Drivers

The critical requirements guiding the design process of one or more subsystems in a mission are known as mission drivers. For the Jason-2 mission, the following drivers have been identified:

- **Jason-2's orbit shall match the operating orbit of Jason-1.**

The Jason-2 satellite needs to follow the same ground tracks as Jason-1 to extend the time series of the measurements. This affects the choice of the launch site, vehicle, time window and orbit maneuvers.

It is well recognized that the usefulness of any altimeter data only makes sense in a multi-mission context (T/P, Jason-1, Jason-2)[7]. In fact, one major objective of this mission is to provide reliable data to be compared with the ones of its predecessors. A direct-comparison of data can, therefore, only be achieved by placing the satellites in an identical orbit under the same conditions. Calibration is crucial to get comparable data and establish a long data record for global climate change studies; this is possible making nearly simultaneous measurements of the same sea-surface from the same altitude.

- **The measurements shall maintain or improve Jason-1's accuracy.**

The sea-surface height shall be provided with a globally averaged accuracy of at least 3.4 cm[10] and the spacecraft shall have a pointing accuracy of 0.15°[17]. This conditions the instrument's selection and the performance of the attitude control system.

The accuracy of TOPEX/Poseidon, Jason-1 and Jason-2's measurements was unmatched by any other altimetry mission at the time. At global and oceanic scales, these missions were the only one accurate enough to detect global ocean changes in time [68]. High-accuracy measurements into multiple decades have been recognized as crucial when integrating long-term climate prediction models [68]. A failure in the completion of this driver would compromise the whole scientific research.

## 4 Functional Analysis

The goal of the functional analysis shown in Figure 1 is to identify the functions the system has to perform in order to successfully carry out the mission avoiding any redundancy. By decomposing these functions, it is possible to highlight the principal operations and to order them in a logical sequence.

The dashed parts represent those functions which were not planned when the mission was first designed but were implemented later on during the operations.

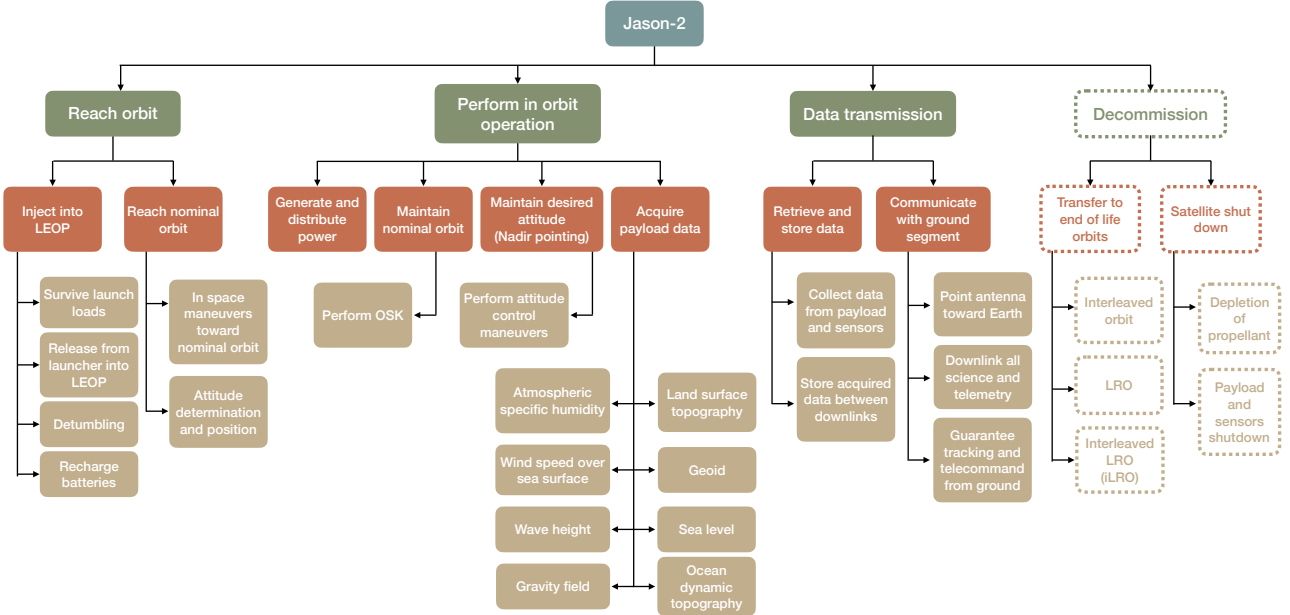


Figure 1: Functional analysis.

## 5 Mission Phases and Correlation to Functionalities

The OSTM/Jason-2 mission is divided into seven phases that overlap each other.

Since the OSTM/Jason-2 satellite was designed and built prior to the implementation of the NASA standard 8719.14 (August 2007), the mission did not comply to the requirement for all spacecraft operating in LEO that limits the disposal phase to a maximum orbital life time of 25 years [98].

Because of this, the disposal was not considered as a phase during the mission design. It is however here presented, as it was later on executed.

### 1. Launch and Early Orbit Phase

Jason-2 is launched and placed into an initial LEOP. The satellite and its instruments are activated and checked out.

Launch was performed on June 20, 2008 and placed the satellite about 10 to 15 km below Jason-1's orbit, with a lag inferior to 10 minutes. Solar arrays were deployed, instruments were powered up, and Poseidon 3 was rotated to have nadir-pointing [68].

### 2. Orbit Acquisition Phase

The satellite is gradually maneuvered into its operational orbit.

Thrusters were used to perform in space maneuvers and reach the nominal orbit at the same elevation as Jason-1. The lag between the two satellites was reduced to 55 seconds [7].

### 3. Assessment Phase

Instrument systems are functionally certified and the ground system is ready to operate regularly.

From the end of Early Orbit Phase, Jason-2 instruments measurements were constantly transmitted to the ground segment in order to assess their correct functioning and verify that the satellite is in its operational orbit.

### 4. Verification Phase

Instruments and data processing algorithm are validated and calibrated. After Jason-2 reached its nominal

orbit and the satellite along with its sensor systems were functioning normally, ground data and laser ranging data were collected and verified. Station keeping and attitude control maneuvers were continuously performed to maintain the desired measurement precision.

Two verification workshops were held in November 2008, and June 2009, to validate near real time products (OGDRs) and off-line products (IGDR, GDR) respectively [10].

## 5. Initial Routine Operations Phase

Instrument data are collected and monitored continuously.

This phase began after the completion of the Assessment Phase and was set to last for three years after launch. Ocean surface topography measurements were acquired and simultaneously corrected by primary payload.

## 6. Extended Routine Operations Phase

Assuming that useful data continues to be collected, this phase extends the mission of two years or an additional period selected by the mission partners.

In 2011, NASA recommended an extension of the mission until 2013, which was then extended for an additional two years. At the end of this period, CNES and EUMETSAT approved an extension up to 2017. To complement Jason-3, operational since July 2016, the Jason-2 mission was lastly extended until 2019 [17].

## 7. Decommissioning Phase

Jason-2 is moved from its nominal orbit while still performing measurements and ultimately shut down. During the mission the spacecraft was moved to an interleaved orbit, which was then followed by two drifting orbits to minimize risk and avoid constellation deployments [8].

Final decommissioning activities were performed after mission formally ended in 2019 by depleting the remaining propellant, powering off all sub-systems, and disconnecting the solar arrays to let the batteries run down [28].

# 6 Concept of Operations

The mission ConOps are summarized in Figure 2<sup>1</sup>. Station-keeping maneuvers and communication with ground station were not continuous operations, therefore the period in which they are carried out is shown. Black lines represent operations performed once during the main phases.

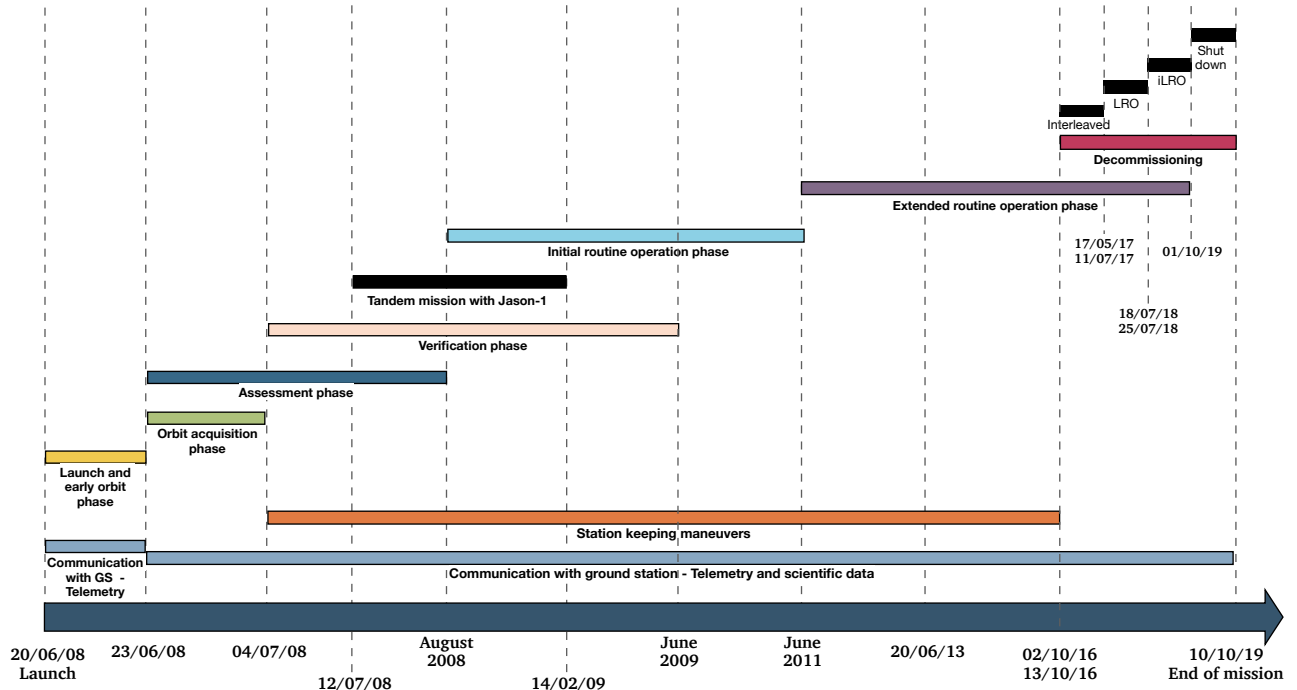


Figure 2: Mission Conceptual Operations.

<sup>1</sup>Not to scale

## 7 Goal-P/Ls Functions Correlation

### 7.1 Main Payloads Overview

In order to accomplish the mission goals, Jason-2 was equipped with five payload instruments with the same functionalities as the ones of Jason-1 but enhanced in performance and reliability. [24]



Figure 3: Main P/Ls disposition in S/C.[10]

1. **Poseidon-3 (Solid-State Radar Altimeter)**: the main instrument of the Jason-2 mission. This is a two-frequency nadir-pointing radar altimeter whose main function is to chart the topography of the sea surface. The instrument computes the ocean surface current velocity in order to evaluate both the wave height and the wind speed. It also possesses an experimental mode allowing the instrument to gather measurements on rivers, lakes and near coastal areas;
2. **AMR (Advanced Microwave Radiometer)**: This radiometer detects the brightness temperatures in the nadir column via three separate frequency, 18.7, 23.8 and 34 GHz[10][17]. Measurements acquired at each frequency are combined to determine atmospheric water vapor and liquid water content. The main function of this instrument is to correct the measurements made by the altimeter by converting the brightness temperatures in an information on the path delay.
3. **DORIS (Doppler Orbitography and Radiopositioning Integrated by Satellite)**: The DORIS package's main function is to provide position and ionospheric correction and, thus, a precise orbit determination to Poseidon-3. It consists in a dual-frequency instrument able to determine atmospheric electron content.  
The whole system is divided into an onboard package, a network of around 50 beacons around the world and a ground system[17]. During its orbit, the beacons record the satellite's location. Once the spacecraft flies over a beacon, a signal is sent at two different frequencies to the receiver. The instrument measures the shift in the frequency for both frequencies between the signal sent and received. The orbit ephemeris is then computed onboard with a precision of 1m.
4. **GPSP (Global Positioning System Payload)**: The GPSP is a tracking system that receives dual-frequency navigation signals continuously and simultaneously from 16 GPS satellites to determine the accurate position of the transmitter [72]. GPSP is a fully redundant unit with an omnidirectional antenna, a low-noise amplifier, a crystal oscillator, a sampling down converter, and a baseband digital processor assembly, all communicating through a 1553 bus interface [17]. It supplies additional positioning data to DORIS in support of the POD function and enhances and/or improves gravity field models.
5. **LRA (Laser Retroreflector Array)**: It is a totally passive unit, placed on the nadir face of the satellite. The LRA is an array of mirrors that provides a target for laser tracking measurements from the ground. By analyzing the round-trip time of the laser beam, it is possible to locate where the satellite is on its orbit. Laser tracking data are analyzed to calculate the satellite's altitude to within a few millimeters. However, this solution cannot track the satellite continuously because of the few ground stations available and the laser beams sensitivity to weather conditions. Other onboard location systems are thus needed. LRA provides a reference target for SLR measurements, which are necessary to calibrate the POD system and the altimeter throughout the mission.

## 7.2 Mission Goals-P/Ls Functions Correlation

The instruments onboard the satellite can be divided in two categories: those performing the measurements to fulfill the scientific objectives and the ones responsible of correcting them. Poseidon-3, assisted by AMR, handles the acquisition of ocean surface topography data. The rest of the payloads improve measurements accuracy by collecting data for POD. Further explanation is presented in Table 1:

Payloads for Scientific Objectives		
Instrument	Functions	Goals to achieve
Poseidon-3	<ul style="list-style-type: none"> <li>- Measure sea-level height</li> <li>- Compute ocean surface current velocity</li> <li>- Evaluate wave height</li> <li>- Evaluate wind speed</li> </ul>	<ul style="list-style-type: none"> <li>- Acquire ocean surface topography measurements</li> <li>- Compute high precision altimetry of sea level</li> <li>- Acquire measurements near coastal zones, rivers and lakes</li> </ul>
AMR	<ul style="list-style-type: none"> <li>- Measure the brightness temperature in the nadir column</li> <li>- Measure water vapor content</li> </ul>	<ul style="list-style-type: none"> <li>- Provide path delays correction to the Poseidon-3</li> <li>- Provide a correction for non-raining clouds</li> <li>- Provide correction for effects of wind-induced enhancements in the sea-surface</li> </ul>
Payloads for Correction		
Instrument	Functions	Goals to achieve
DORIS	<ul style="list-style-type: none"> <li>- Measure the shift of frequencies between the sent and received signal</li> <li>- Determine atmospheric electron content</li> </ul>	<ul style="list-style-type: none"> <li>- Provide ionospheric correction</li> <li>- Provide real-time location and precise orbit determination</li> <li>- Perform geophysical studies</li> </ul>
GPSP	- Receive navigation signals from 16 GPS satellites	<ul style="list-style-type: none"> <li>- Provide supplementary satellite data</li> <li>- Improve gravity field models</li> </ul>
LRA	- Analyze the round-trip time of a laser beam signal	<ul style="list-style-type: none"> <li>- Calibrate the POD system and the altimeter</li> </ul>

Table 1: Goal-to payloads functions correlation.

## 7.3 Additional Payloads

In addition to the main payloads described above, OSTM/Jason-2 includes three experimental passenger instruments whose goal is to perform complementary measurements to further improve the accuracy of onboard primary devices. These instruments need to be taken into account due to their particular influence on the design of EPS, TCS, OBDH and configuration.

- **CARMEN-2 (Environment Characterization and Modelisation-2)**

This instrument studies the effects of radiation in the satellite's environment on advanced components. In particular, it measures electrons, protons and ion fluxes in the energy ranges responsible for component damages, in order to define associated effects on test components, characterize the local radiation environment for DORIS and evaluate its potential drifts inside the SAA[17].

- **LPT (Light Particle Telescope)**

This instrument studies radiation in the satellite's environment and complements the radiation measurements of CARMEN-2. The observed data improves and characterizes the local radiation environment to evaluate errors of other mission instruments.

- **T2L2 (Time Transfer by Laser Link)**

T2L2 refers to detectors for ultra-precise time transfer, it uses a laser link to compare and synchronize remote ground clocks with high accuracy. The T2L2 system on Jason-2 allows the precise characterization of the positioning system of DORIS.

## 7.4 P/Ls - ConOps/Phases Correlation

A correlation between P/Ls and ConOps/phases is delineated below:

- **Poseidon-3 (Solid-State Radar Altimeter)** is rotated towards Nadir during the Launch and Early Orbit phase and activated when the Orbit Acquisition phase comes to an end on July 4, 2008 [8]. The data is analyzed and monitored to calibrate and validate the accuracy of the measurements during the Assessment phase and the Verification phase. It then stays operational acquiring data for the time of the Initial Routine Operations phase and Extended Routine Operations Phase. It remains operative throughout the different orbits (interleaved, RLO,iRLO) until the complete disposal phase terminates.

- **AMR (Advanced Microwave Radiometer)** is switched on at the end of the Orbit Acquisition phase. It is checked and validated along the Assessment phase and Verification phase. It continues to improve Poseidon-3's measurements for the Initial Routine Operation Phase and the Extended Routine Operations Phase.
- **DORIS (Doppler Orbitography and Radiopositioning Integrated by Satellite)** is activated in the Launch and Early orbit phase and it is used to pinpoint the satellite's location in orbit. It is checked and validated during the Assessment phase and Verification phase and it operates throughout the Initial Routine Operation Phase and the Extended Routine Operations Phase.
- **GPSP (Global Positioning System Payload)** is switched on during the Launch and Early orbit phase and it assists DORIS in the orbit determination of the satellite. It is calibrated during the Assessment phase and Verification phase. It is operative during the Initial Routine Operation Phase and the Extended Routine Operations Phase.
- **LRA (Laser Retroreflector Array)** is turned on during the Launch and Early orbit phase and it calibrates the other two location systems. It is checked and validated during the Assessment phase and Verification phase and it operates throughout the Initial Routine Operation Phase and the Extended Routine Operations Phase.

## 8 Mission Analysis Understanding

### 8.1 Trajectory Design

OSTM/Jason-2's trajectory stems from the needs of the mission to cover 90% of the globe's oceans and sample altimetric data with great precision [3]. The orbit is engineered in order to trade off the required accuracy and reduce to a minimum the interactions with the Earth's atmosphere and gravitational field. In addition to this, the launch window was constrained by the necessity to place Jason-2 in the proper orbit plane. The launch occurred in concurrency with a minimum in the solar cycle [73].

- **LEOP**

OSTM/Jason-2 was launched by a two-stage Delta II 7320 rocket on the June 20, 2008. The launch time was arranged to place the satellite in an orbit as close as possible to the nominal one, but on the same plane in order to reduce the  $\Delta V$  required to reach the operational orbit [69]. Jason-2 was injected after 55 minutes into a LEOP, which was about 10-15 km below the nominal one, and the time lag between the two was less than 10 minutes.

The satellite departed from this orbit by performing a shape change maneuver with its thrusters and, then, reached its nominal orbit to start the scientific mission.

- **Nominal orbit**

The operational orbit is characterized by the following orbital elements while the ground track is represented in Figure 4:

a [km]	e [-]	i [deg]	$\Omega$ [deg]	$\omega$ [deg]
7714.432	0.000098	66.042	90.0	116.56

Table 2: Mean classical orbit elements[10].

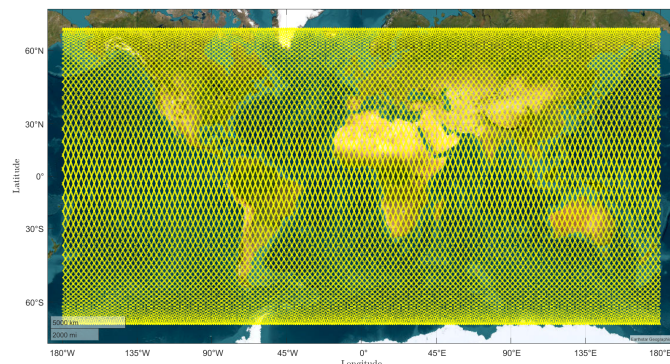


Figure 4: Nominal orbit ground track (10 days, 127 revolutions).

Jason-2 lies on a prograde circular, non sun-synchronous orbit with a ground track repeatability of  $\pm 1$  km cross-track at the equator every 9.9156 days. Furthermore, the choice of the inclination allows for a latitude coverage of  $\pm 66.042^\circ$ [3].

During the first cycles, the tandem mission with Jason-1 is initiated as Jason-2 trails its predecessor by 55 seconds; this allows for a direct comparison and calibration of Jason-2 instruments. Once this mission is completed, Jason-1 will depart from the operational orbit of Jason-2.

In the long term, the instabilities related to the Sun's cycle (Earth's atmosphere and magnetic field) and the perturbations related to air drag, Earth's gravity field and solar radiation pressure, require orbital maneuvers to be carried out every 40 to 200 days. Moreover, each maneuver lasts 20 to 60 minutes and they are preferably performed at the end of each orbit cycle, above the ground stations, to minimize lost data acquisition time [3].

- **Decommissioning orbits**

Since the extension of the mission, Jason-2 kept operating in its nominal orbit until its successor, Jason-3, was injected in its same orbit and became operational on October 14, 2016. By that time, Jason-2 was moved into an Interleaved orbit where it kept sampling useful data.

In 2017 the degradation of critical onboard components and control systems led the mission partners to move Jason-2 to the LRO where it kept providing valuable oceanographic measurements and science observations on a grid covering the whole globe with only four kilometers separation at equator in this 1309.5 km orbit [21].

Lastly, on July 25, 2017 Jason-2 was moved to the iLRO, where, thanks to another year of complete measurements, it was able to provide data on a 4 km resolution grid.

## 8.2 Functionalities-Phases Correlation to Trajectory Design

Table 3 shows how the functionalities constrained the characteristics of the different orbits throughout the mission:

Orbit	Functionalities	Orbit design	Mission Phase
<b>LEOP</b>	Inject satellite from launcher close to nominal orbit	10-15 km below nominal orbit (coplanar)	Launch and Early Orbit Phase Orbit acquisition Phase <sup>2</sup>
<b>Nominal</b>	Study of ocean variability	9.9156 days groundtrack repeat cycle	Orbit acquisition Phase Assessment Phase Verification Phase Initial Routine Operations Phase Extended Routine Operations Phase
	Acquire vast ocean surface topography	Orbit inclination of $66.042^\circ$	
	Acquire orbit knowledge for precise data acquisition	1136 km height to minimize disturbances due to Earth's atmosphere and gravity field	
	Avoid aliasing in tide readings	Prograde and not sun-synchronous orbit[3]	
	Sample accurate altimetric measurements	Low eccentricity of 0.00098	
	Communicate with ground station	Orbit designed to pass over dedicated ground calibration sites <sup>3</sup>	
<b>Decommissioning</b>	Minimize risk and avoid constellation deployment	"Graveyard" orbit of height 1309.5 km with a drift of 40 m/year [28]	Decommissioning Phase

Table 3: Functionalities-phases trajectory design correlation.

<sup>2</sup>Orbit Acquisition Phase starts in LEOP and finishes when reaching nominal orbit

<sup>3</sup>Cape Senetosa in Corsica and Harvest Oil Platform in California USA

# Homework 2

## Mission Analysis & Propulsion Subsystem

Change log	
§ 2.3	p. 13: changed comparison to monopropellants only; new table and comments added
§ 2.4	p. 13: introduction changed p. 14: table 6 and table 8 revised and commented p. 15: table 9 revised and commented; table 10 revised
§ 2.5	p. 16: table 12 revised; extended budget comments

# 1 Homework 2.1

## 1.1 Mission trajectory design

The trajectory of Jason-2 satellite is designed to ensure a successful acquisition of the operational orbit to fulfill the mission's observation objectives. In particular, a sequence of initial maneuvers is performed to achieve the right phasing with Jason-1 satellite to properly cross-calibrate altimeters during tandem-flight operations. Failure to fulfill these requirements would compromise the results of the entire satellite series.

The design is fully dependent on the date of launch as it defines the number of rendez-vous maneuvers and the duration of the orbit acquisition phase. Once the launch date is set, the nominal trajectory is designed so that, after the Early Orbit Phase where Jason-2 is inserted into a LEOP, a series of three SMA RV maneuvers are performed to complete the Orbit Acquisition Phase. These maneuvers precisely position Jason-2 so to start the Verification phase. From the moment Jason-2 reaches the nominal orbit, it performs station keeping maneuvers to comply with the measurements accuracy requirements. During the Initial Routine Operation Phase and the Extended Routine Operation Phase no other significant maneuvers are performed until decommissioning. During the entire life of the satellite no collision avoidance maneuver have been necessary [38].

- **LEOP:** The Launch and Early Orbit Phase is successfully completed once Jason-2 reaches the LEOP which is 10 km below the nominal orbit. This avoids polluting the operational orbit with unwanted debris from the launcher and creates a drift to reach the right time phase between Jason-2 and Jason-1. From the LEOP, a first test manoeuvre of minor entity ( $\Delta V < 15 \text{ cm/s}$ ) is performed to check the propulsion system as part of the Assessment Phase operations followed by the first SMA RV whose cost is expected to be less than 5 m/s.[79] [75] These maneuvers lead to a change in altitude of about 10 km. A second SMA RV maneuver ( $\Delta V < 5 \text{ m/s}$ ) further increases the altitude by another 10 km, positioning the satellite above the nominal orbit to await for a safe position relative to Jason-1. Upon reaching the nominal orbit on July 4, 2008, through the last SMA RV maneuver ( $\Delta V < 5 \text{ m/s}$ ), Jason-2 achieves proper phasing with Jason-1, marking the completion of the Orbit Acquisition Phase and the beginning of the Verification Phase. From the beginning of the mission up to 2008, the propellant consumed amounts to 3.5 kg overall. [76]

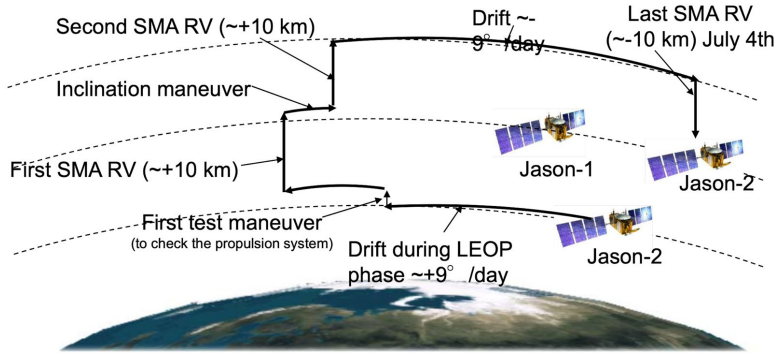


Figure 5: Jason-2 Station Acquisition. [75]

- **Nominal Orbit:** The acquisition of the correct position in the operational orbit allows the beginning of the Tandem Mission with Jason-1 on July 17, 2008 as part of the Verification Phase. Throughout this operation the two satellites' trajectories shall be contained in a 1 km band and shall have a time lag of 55 seconds.[79] [7]

In order to maintain the orbit within  $\pm 1 \text{ km}$  from the reference grid throughout the Assessment Phase, Verification Phase, Initial Routine Operation Phase and Extended Operation Phase, station keeping maneuvers are performed every 40-200 days.

- **Decommissioning Orbits:** On October 2, 2016, after completing the cross-calibration with its successor[9], Jason-2 is moved from the nominal orbit into an interleaved orbit 12 km below. Due to gyro anomalies and global aging of the satellite, it is then maneuvered towards the LRO at 1306.5 km of altitude. The fuel necessary to move the satellite from the nominal orbit to the LRO amounts to 4 kg.[38] In 2018 the satellite was transferred into an iLRO, decreasing its altitude of 250 m consuming 0.55 kg overall. In the same year, 12 kg of hydrazine were depleted to ensure as few propellant as possible left in the tank, once Jason-2 becomes non-operational.[39] On October 1, 2019, due to battery management critical anomalies, it was decided to ultimately dispose Jason-2. [37]

## 1.2 Reverse engineering of $\Delta V$ budget

In order to grasp the entity of the whole  $\Delta V$  and its distribution throughout the mission, a comprehensive analysis was conducted on all maneuvers executed. The initial SMA RV and the station keeping manoeuvres were evaluated separately. The study spanned over a period of 5 years: 3 years for the nominal mission and the 2-year extension that was already accounted for during the design process.[68] Any further extension of the Extended Routine Operation Phase and the Decommissioning phase were omitted from the breakdown of  $\Delta V$ , as they were not part of the pre-launch planning.

- **Orbit Acquisition Manoeuvres**

The cost associated to the Orbit Acquisition Phase was estimated by evaluating three different Hohmann transfers. The initial idea of using Lambert's arcs to model the transfers was abandoned due to the inconsistency of the results which were significantly overestimated ( $\sim 8000$  m/s). The discrepancy is due to the lack of information on the correct time of flight to be set as input to the Lambert Problem. The Hohmann transfer was then chosen as the most intuitive alternative, given that the manoeuvres occur between two approximately circular and co-planar orbits.

The change of inclination was not considered due to its magnitude being on the order of  $10^{-3}$  degrees [69], thus having a minor impact on the total manoeuvre cost compared to the change of semi-major axis.

- **Station keeping**

The orbit maintenance manoeuvres were evaluated hypothesizing Lambert transfers in a non stochastic manner. Their cost was derived analytically by combining the data retrieved from the ephemerides and the Table of Events. [69] [32]

The simulation consisted in computing the  $\Delta V$  for each manoeuvre listed in the Table of events, which precisely documented the initial and final time of the manoeuvre. It was then possible to extract the Cartesian coordinates from the ephemerides at the beginning and at the end of each manoeuvre. From this data, it was possible to implement a Lambert Problem, with a TOF equivalent to the duration it took for the satellite to complete the manoeuvre. [86]

## 1.3 $\Delta V$ budget breakdown and margins

A breakdown of the results computed is shown in Table 4 and compared with the real fuel consumption which is the real fuel mass consumed, retrieved from the official reports ([75] and [78]).

The ESA Standard Margin Philosophy Description<sup>4</sup> was chosen to reconstruct the margin on the the total  $\Delta V$  computed. Since both the orbit acquisition and the OSK maneuvers were accurately computed from the simulation, an appropriate margin was identified in MAR-DV-010. [20]

This resulted in an addition of 10 m/s to the total  $\Delta V$  budget, being more than the 5% of the value (1.25 m/s) in accordance with normative.

The logic behind the computation of the consumed fuel starting from the  $\Delta V$  budget is explained in subsubsection 2.4.1.

Year	Number of Manoeuvre	Maneuver Mean Duration	Computed Total Cost [m/s]	Computed Fuel [kg]	Real Fuel Consumption [kg]
2008	1-3	171 min	14.100	3.3	3.5
	4-6	52 s	1.414	0.33	
2009	7-9	52 s	1.447	0.34	$\sim 0.3$
2010	10-11	52 s	1.050	0.25	<sup>5</sup> N/A
2011	12-16	52 s	2.360	0.55	N/A
2012	17-21	52 s	2.528	0.59	N/A
2013	22-27	52 s	2.107	0.49	N/A
Total Cost			25.006	5.85	N/A
Total costs with margins			35.006	8.70	N/A

Table 4: Table of  $\Delta V$  budget breakdown.

<sup>4</sup>ESA Standard Margins are applied even if the mission is a collaborative effort of NASA, CNES, NOAA, EUMETSAT

<sup>5</sup>Affected by too high uncertainty

## 2 Homework 2.2

### 2.1 Mission propulsion architecture

To understand Jason-2's mission propulsion architecture it is important to consider that, just like its predecessor Jason-1, the satellite utilized a multi-mission platform provided by CNES and TAS known as PROTEUS.[10] This platform provided all the housekeeping functions including the propulsion system. [65]

PROTEUS has an independent propulsion module with a hydrazine monopropellant blow down system; composed of a hydrazine tank, four thrusters (with their valves), a pressure transducer, a propellant filter, two fill and drain valves, and a latch valve. [65] An overview of this propulsion sub-system is shown in Figure 6a.

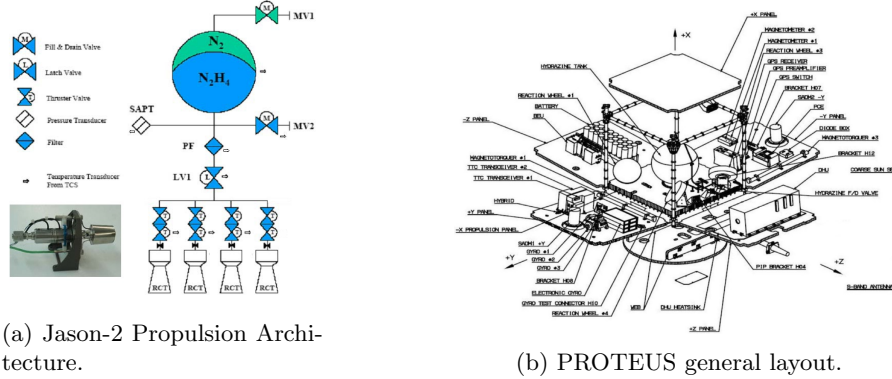


Figure 6: Architecture of Jason-2's Propulsion.

- **Hydrazine tank**

The hydrazine monopropellant unit includes a Positive Expulsion Propellant Tank (PEPT) by RAFAEL (Israel) made of two 6Al-4V titanium alloy thin-walled hemispheres, pressurised with gaseous nitrogen. [87] This 37.5 L tank is located at the centre of the platform module to protect it from possible debris impact and for inertia considerations. [36]

The operating pressure range goes from 25.4 to 5.5 bar and the operating temperature extends from 4° to 55°. The hydrazine nominal capacity has a maximum of 30 kg, that reduces to 28 kg at a 4:1 blow-down ratio. [87]

The positive fluid expansion is provided by an EPDM rubber diaphragm, that has the role of allowing active and efficient propellant management throughout the satellite's lifetime. [87] This can prevent undue sloshing loads, ensure consistent propellant feed, and minimize centre of gravity shifts; factors that remove limitations caused by the satellite orientation or movements, and contribute to a better stability for in-space. [73] After Jason-1, the use of hydrazine tank raised NASA concerns for possible leaks that pose a danger for satellite integration teams. Because of this, CNES decided to weld the hydrazine tank segments for the Jason-2 missions.

- **Thrusters**

Orbit adjustments manoeuvres were executed by Jason-2 by firing any combination of its four on-board thrusters that were installed on the -X face of the satellite, as shown in Figure 6b. [30]

Each monopropellant hydrazine thruster, provided by EADS-ST, had a thrust of 1 N and a nominal specific impulse of 220 s.[1][74] The thrusters were equipped with a flow control valve to control their propellant supply, and an internal catalyst bed heater with thermal insulation for the decomposition of hydrazine.

The 1 N thrusters are designed for both, long term steady state and pulse mode operation; they also operate in a wide pressure range which makes them ideal for blowdown propulsion systems. The thrusters are qualified to withstand sinus and random vibration.[1]

- **Valves**

On top of the valves in the thrusters, Jason-2's propulsion system was also equipped with two fill and drain valves and a latching valve. The first two are composed by three mechanical barriers, whilst the latch valves provide an additonal mechanical barrier to meet the launch safety requirements.[87]

- **Pressure Transducer**

Usually, pressure transducers were not included for hydrazine propulsion; however, Alcatel Space added one in the subsystem architecture to have a better accuracy for filling,  $\Delta V$  measurements and to monitor the tank state throughout the whole mission. The pressure accuracy for the Jason-2 mission was of 0.2% full scale.[65]

## 2.2 Primary and secondary propulsion

According to the literature definition of primary and secondary propulsion units, the propulsion subsystem on board Jason-2 mission should be considered a secondary propulsion unit.[29] As a matter of fact, the main functions carried out by the propulsion subsystem of Jason-2 are station keeping, semi-major axis rendez-vous in space and minor orbital parameter changes. It is however of poor meaning to define a secondary system without the primary one. For this reason, in this case, there is little point in identifying a primary or secondary subsystem, being the only one on board.

The propulsion choice is strongly related to the functions that the satellite has to perform and the environment in which it operates. For Jason-2, no major orbit changes are required to accomplish the mission as the insertion into the nominal orbit does not require any dramatic change of the Keplerian elements. When on the operational orbit, only station keeping maneuvers are carried out in order to keep Jason-2 in a  $\pm 1$  km range with respect to the reference nodes. [75] Furthermore, the nominal orbit is engineered to minimize the interactions with the Earth's atmosphere and its gravitational field.[3] All in all, in light of the analysis, the required centre of mass corrections lead to the choice of a secondary propulsion unit.

## 2.3 Justification of propulsion type and architecture

As part of the PROTEUS family, Jason-2 was equipped with a monopropellant liquid hydrazine propulsion system. The main drivers in the choice of this propulsive unit were the simplicity and compactness of the overall system, as a particularly high specific impulse was not required. In fact, with this configuration, only one tank and one feeding system are needed.

To justify the use hydrazine, a comparison with other monopropellants was conducted. The different types, along with their respective density, specific impulse, and other properties, are shown in Table 5.

	Hydrazine (N <sub>2</sub> H <sub>4</sub> )	Nitrous Oxide (N <sub>2</sub> O)	Hydrogen Peroxide (H <sub>2</sub> O <sub>2</sub> , 80%)
Density [kg/m <sup>3</sup> ]	1020	1977.7	1388
Specific impulse [s]	191	152.7	160
Operating temperature [K]	896	1609	1274
Physical properties	Liquid colorless, toxic and flammable	Self-pressurizing, colorless gas	Liquid colorless, burns skin and flammable

Table 5: Monopropellants comparison.[61]

As shown above, despite its toxicity, hydrazine proves to be the best option. This is because it is characterised by the highest specific impulse and the lowest operating temperature. The lower temperature allows the use of low cost materials.[22] Despite nitrous oxide outperforming hydrazine in terms of volumetric specific impulse, its high operating temperature makes it less suitable for this mission. In addition to this, unlike hydrogen peroxide, which is affected by a slow decomposition (about 1% per year), hydrazine is stable and therefore storable for long periods if kept in the correct conditions.[61] Hydrazine also has a greater heritage in space applications, including the preceding mission Jason-1.

Regarding the architecture, the four thrusters used for propulsion are mounted on the -X face of the satellite to avoid interference with the precise measurements of the payloads. During the initial and orbit acquisition phases maneuvers, all four thrusters are employed to produce thrust. Differently, station-keeping maneuvers are performed with a combination of the four.[68]

## 2.4 Reverse sizing

The propulsion subsystem was sized through reverse engineering to help understand and justify design choices. The sizing of the propulsive subsystem is carried out following the procedure described in the following sections. Starting from the  $\Delta V$  value of 130 m/s retrieved from the real platform's data-sheet of the Jason-3 mission, a margin of 100% has to be applied to this  $\Delta V$  value.[40][20] Hence, 260 m/s.

### 2.4.1 Propellant selection and masses

The mass of propellant needed on board can be computed from the  $\Delta V$  budget of the mission and the dry mass of the satellite. According to planetary satellite data, the nominal dry mass of the S/C can be determined from the payload mass. For a P/L mass of 120 kg [10], linear regression shows a dry mass of 420 kg.[55] Including a 20% system margin, (MAR-MAS-040), required by ECSS, the adjusted dry mass amounts to 504 kg. This value is comparable to the real dry mass  $m_{dry} = 525$  kg [10] committing a relative error of 4%.

Inverting the Tsiolkovkij equation and knowing that the  $I_{sp}$  of the thrusters is 220 s [1], the value of the MR and consequently the amount of propellant discharged to complete each maneuver can be calculated. In addition, a margin of 3% is added to take into account ullage, a 2% margin for residuals (MAR-MAS-080) and 0.5% for the loading uncertainty. The obtained result is shown in Table 6 along with the error with respect to the real case.

Real Propellant Mass [kg]	Propellant Mass [kg]	Error
28.3	68.10	+141%

Table 6: Computed propellant masses and errors.

It can be observed that a low correspondence is shown with the real data[17]. This was to be expected due to the impact of the high margin considered on the  $\Delta V$ .

#### 2.4.2 Tank Sizing

The pressurizing system of the Jason-2 satellite uses a blowdown architecture. Nitrogen (N2) is used as a pressurizing gas.

Given the numerous unknowns in our sizing process and the sole provided value of the blowdown ratio from the datasheet [87], the procedure adopted for the sizing of the tank and feeding line is as follows.

The value of the pressure inside the thrusters was arbitrarily set within the constraints specified in the datasheet [74], while the pressure inside the tank was iterated within the ranges available on the datasheet. [87][1] The pressure inside the tank, in fact, needs to fulfil some constraints so that the architecture is physically admissible:

1.  $P_{tank,fin} > \Delta P_{feed} + P_{thrusters}$

The pressure inside the tank when almost all the fuel is depleted needs to be compensated for the inlet pressure of the thruster and the pressure losses inside the pipes.

2.  $P_{tank,in} \in [5.5, 25.4]$  bar and  $P_{tank,fin} \in [5.5, 25.4]$  bar

The pressure inside the tank should always be comprised with the nominal values from datasheet. [87]

This iteration generated a wide array of combinations. Knowing that the typical value for pressure variation in the feeding lines of space applications has a value of 50 kPa, the combination of values yielding a  $\Delta P$  closest to this standard was selected.

$P_{tank,in}$ [bar]	$P_{tank,fin}$ [bar]	$P_{inlet}$ [bar]	B [-]
24.00	6.00	5.5	4

Table 7: Pressure conditions and blowdown ratio.

With the knowledge of the computed mass of propellant and the density of hydrazine, it is possible to compute the volume of propellant. A margin of 10%, (MAS-CP-010), of unusable volume is added. To compute the total tank volume, it is necessary to know the initial volume of the pressurising gas. To calculate it, an isothermal transformation is assumed. This hypothesis is valid for slow expansions as for slow discharges, like in blowdown systems. Thus, the initial volume of the pressuring gas is  $V_{gas,in} = \frac{V_{prop}}{B-1}$ . Finally, the volume of the tank is the sum of the initial volume of the propellant and of the pressurant gas.

A summary of all the values found is presented in Table 8.

$V_{gas,in}$ [L]	$V_{gas,fin}$ [L]	$V_{tank}$ [L]
24.72	98.90	99.88

Table 8: Tank volume values.

From the real mission data, the volume of the tank is 37.5 L[17], which leads to an error of +166 % with respect to the computed one. Once again, this is due to the high margin applied to the  $\Delta V$ .

The tank is spherical and the material is Ti-6Al-4V. The choice of the tank is constrained by the solution adopted by the PROTEUS platform that englobes a spherical tank with pre-defined shape size and mechanical properties.

The diameter of the tank is computed by knowing the volume of the tank. The thickness derives from the formula  $t = \frac{r_{tank} \cdot P_{max}}{2 \cdot \sigma}$ . The mass of the tank is computed considering the tank as a hollow sphere of thickness t and of density  $\rho_{tank} = 4420 \text{ kg/m}^3$ .[87] The choice of the ultimate tensile strength is related to the maximum pressure before burst and through a correction factor of 1.5, leading to the value of  $\sigma = 880 * 10^6 \text{ Pa}$ .[87][71]

Diameter [mm]	Thickness [mm]	Tank Mass [kg]
573.75	1.42	6.54

Table 9: Structural Properties of the tank.

The actual diameter and tank mass are 420.0 mm and 3.90 kg, respectively [87]. The computed values show errors of +37% for the diameter and +68% for the mass compared to the real values.

The tank on board Jason-2 is made out of Ti-6Al-4V. The reason behind this choice is that for hydrazine propellant, the best compromise between decomposition rate, self-passivation and metal dissolution can be achieved through the use of Ti-6Al-4V.[5] Ti-6Al-4V also has a lower ratio  $R$  of density over yield strength than Aluminium ( $\frac{\rho_{Ti-6Al-4V}}{\sigma_{Ti-6Al-4V}} = 4.58 \text{ kg/m}^3/\text{MPa}$  compared to  $\frac{\rho_{Al}}{\sigma_{Al}} = 5.59 \text{ kg/m}^3/\text{MPa}$ ). Thus, for the same mechanical performance, the mass of the tank with Ti-6Al-4V is lower than with an Aluminium alloy.

#### 2.4.3 Pressurant selection and masses

The pressurizing gas is used to push the propellant towards the engine during flight, ideally it needs to be a lightweight and inert gas. The pressurant gases that can be used for PEPT-420N tank are either helium ( $He$ ) or nitrogen ( $N_2$ ) and as such a comparison for these two gases will be made.[87]

The mass of the gasses is computed by using the ideal gas equation considering that the gas is at  $T_{tank} = 293 \text{ K}$  which is within the nominal temperature range. [87] A 20% margin (MAR-MAS-090) has been added to the mass, as it is the standard for pressure-fed systems. The results are contained in the following figure:

Mass of $He$ [kg]	Mass of $N_2$ [kg]
0.117	0.819

Table 10: Mass of pressurants.

Despite helium would seem preferable to nitrogen in terms of mass, the reasons why the second was chosen as pressurant gas may be several.

In the first place, nitrogen is more abundant and less expensive than helium. For large-scale space projects, which often operate under strict budget constraints, cost-effectiveness can be a significant advantage.

Nitrogen also has favorable storage and transportation characteristics. The smaller atomic size of helium makes it more prone to leakage. Nitrogen's larger molecule size mitigates this risk, ensuring more reliable storage and reducing the potential for loss during transportation to and within the space environment.

Overall the performance of nitrogen in space application may be more predictable based on several past mission experience.

#### 2.4.4 Feeding strategy selection and sizing

Considering the values of the volume and pressure of the tank used in the mission, from statistical regression data of Figure 7 it is possible to deduce that a pressure-fed architecture system is more suited to our problem.

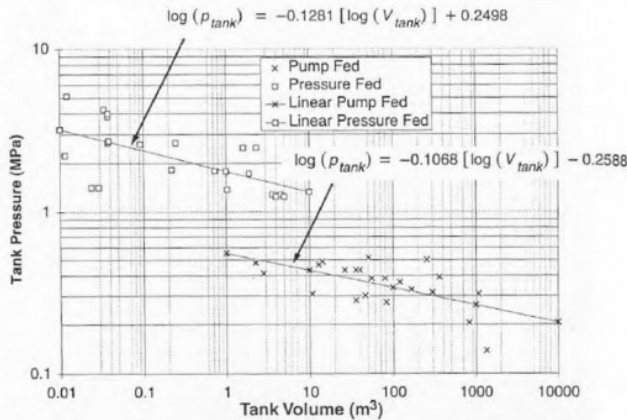


Figure 7: Pressure-fed vs Turbopump-fed. [60]

Pressure fed system is mostly implemented with low tank volumes. It is largely used for its simplicity and low cost which is reflected on the design's architecture and it is regarded for its in space applications such as small orbit manoeuvres, orbit maintenance and attitude control. [29]

On the other hand, turbopumps are generally used with high tank volume at low pressure. This is because turbopumps will increase the pressure of the propellant, thus the gas can be maintained at lower pressures in order to save mass.

In order to size the feeding line between the tank and the thrusters, it is necessary to compute the most important characteristics of the flow in the line as Reynolds number, friction factor and length of the pipes.

The dynamic pressure  $\Delta P_{feed}$  is computed as  $\Delta P_{feed} = P_{gas,fin} - P_{inlet}$  with  $P_{gas,fin} = 6$  bar and  $P_{inlet} = 5.5$  bar. By taking the definition of the dynamic pressure, an approximation of the flow velocity is computed as  $v_{feed} = \sqrt{\frac{2 \cdot \Delta P_{feed}}{\rho_{prop}}}$ . Knowing the dynamic viscosity of hydrazine  $\mu = 0.876 \cdot 10^{-3} \text{ Pa} \cdot \text{s}$  and the dimension of the pipes  $d = 6.25 \text{ mm}$  [87], the Reynolds number is then calculated. The friction factor is estimated using the Moody diagram under the hypothesis of smooth pipe and turbulent flow. Finally, the length of the line is determined as  $L = \frac{\Delta P_{feed} \cdot 2 \cdot d}{f \cdot \rho_{prop} \cdot v_{feed}^2}$ . The results are summarized hereafter:

Flow velocity [m/s]	Reynolds number [-]	Friction factor [-]	Length [m]
9.9572	71752	0.0193	0.3238

Table 11: Feeding lines sizing.

#### 2.4.5 Number and positioning of thrusters

Jason-2 uses a combination of 4 thrusters to perform orbital manoeuvres.

In order to correct a possible misalignment of the centre of mass with respect to the thrust, a minimum number of three thrusters is required. It is likely that the forth thruster was added for redundancy reasons, making it possible to maintain a correctly aligned thrust even if one of the others fails. Since the attitude control is not achieved through the thrusters, they can all be aligned with the direction of motion. [68]

#### 2.4.6 Positioning of tank and lines in the configuration

Jason-2's platform has an overall size of about 1x1x3 m. [68] The configuration of the tanks and the propulsion system is constrained by the implementation of the PROTEUS platform. This platform mounts the tank on the centre of the lower plate, for inertia reasons and to protect it from possible debris impact, and its thrusters under the lower plate, as it can be seen in Figure 6b. This allows to fit both the tanks and the pipelines to feed the thrusters. [90]

### 2.5 Budget

To conclude the propulsion system analysis, the mass and power budgets to effectively perform the required maneuvers are hereby reported:

System mass budget [kg]	System power budget [W]
9.37	96.1

Table 12: System budget mass and power.

It shall be noted that the mass budget of the propulsive subsystem is computed by adding up the tank's mass, the pressurant gas' mass as well as the four thrusters' mass. A 10% margin was included to take into account minor components such as cables, valves and feeding lines.

On the other hand, the power budget for the system is the sum of the required power to manage the thrusters' valves and the catalytic bed.[1] The number and the type of valves were extracted from the general architecture of Figure 6a. The real value for the mass budget retrieved from literature is 18.41 kg[19] which aligns with the 5% of the total dry mass.[55] The computed value is approximately half of the actual value; this discrepancy may be attributed to the lightweight and simple onboard architecture, as well as the applied margins. The computed power accounts for 18% of the satellite's total power budget, which is higher than typically expected for a MetSat. [55]

## **Homework 3**

# **Tracking Telemetry & Telecommand Subsystem**

# 1 TTMTTC Subsystem

TTMTTC (Tracking, Telemetry and Telecommand) is a subsystem of the Jason-2/OSTM spacecraft that focuses on the overall mission management, operations and satellite data reception.[97] This enables full duplex commanding and verification of the satellite's health and status.

## 1.1 Tracking

Tracking involves detecting and reconstructing the satellite state vector for localization and forecast. In the Jason-2 mission, this task is performed by the precision orbit determination system DORIS, with supplementary data from a precision GPS receiver (GPSP) and LRA.

The DORIS system is composed of a ground network of 50 beacons that send signals to the Jason-2 DORIS-DIODE receiver at a frequency of 2.036MHz.[17][68] The receiver is then able to pick up two beacons simultaneously and measure the Doppler shift from the signal sent to generate the orbit ephemerides on-board in real time with a precision of 1 m. The measurements are also sent to the Doris Orbitography Service in Toulouse, where the satellite trajectory and position are calculated.[68]

The GPSP on Jason-2 consists of two independent receivers operating in cold redundancy, each with an omnidirectional antenna, low-noise amplifier, and a baseband digital processor communicating via the bus interface. It is used to validate the measurements and enhance the accuracy of the primary Doris location system data; it is able to track up to 16 GPS satellites simultaneously (3 are the minimum to determine its position) and it makes use of two omnidirectional antennae and low-noise amplifiers.

Lastly, the LRA is another one of the tracking systems onboard of Jason-2; it is placed at the nadir face of the satellite and it provides a reference target for satellite laser ranging (SLR) measurements. The limited number of ground stations and the sensitivity of laser beams to weather conditions make it impossible to track the satellite continuously.

## 1.2 Telemetry and Telecommand

As part of the PROTEUS batch of satellites, Jason-2 ensures the space-ground communication by a S-band TM/TC link. [102] More specifically, the telemetry and telecommand frequencies were selected to be 2215.92MHz and 2040.49MHz respectively.[97] This choice was made taking into account the satellite orbit and the frequencies already attributed, resulting into a band that serves well for this use as it is highly resilient to rain fade and environmental interfaces. [102] [11]

In addition to this, Jason-2 makes use of Solid-State Power Amplifiers, to amplify and direct the downlink signal to the appropriate antenna.

The mission telemetry acquisition strategy is designed to minimise the risk of scientific data losses; this is shown by the fact that in its first years of operations, 99.8% of all available data acquired onboard have been downlinked and archived in Earth mission centers.[79]

Jason-2 telemetry is divided in permanent house-keeping telemetry (HKTM-P), historic house-keeping telemetry (HKTM-R), payload telemetry (PLTM1 and PLTM2) and failure diagnostic telemetry (FDTM), that gives a short-term accurate telemetry before platform failure.[102] In accordance to the CCSDS packet, the previously mentioned streams undergo multiplexing to generate a single stream of data units, which is then downlinked by the satellite antenna (CCSDS).[101] A representation of a general telemetry flow for PROTEUS satellites is shown in Figure 8.

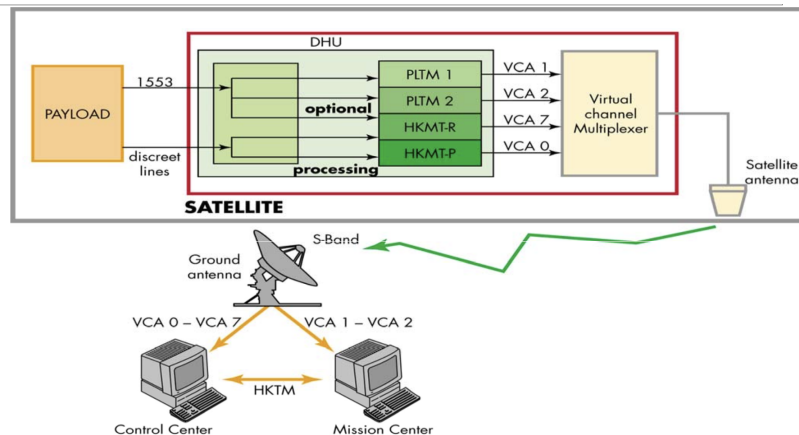


Figure 8: PROTEUS Telemetry flow. [101]

### 1.3 Ground Segment

The Ground System is made up of the ground segments of NOAA, CNES and EUMETSAT. CNES performs satellite analysis, navigation, and POD, whilst maintaining the satellite database. NOAA operates and controls Jason-2 with the support of CNES and NASA/JPL for mission planning and satellite monitoring. EUMETSAT and NOAA receive and store the telemetry and instrument data at their respective ground stations.[97]

Raw telemetry and command data streams are transmitted to/from NOAA's Wallops/Fairbanks Command and Data Acquisition Stations and EUMETSAT's tracking station in Usingen, Germany. [17] This ground station selection is justified by the need of low latency data for marine meteorology applications such as El Niño.

## 2 TTMTTC operations

### 2.1 Phases

- **Launch and Early Orbit Phase:** During launch, the ground segment satellite tracking is enhanced by tracking stations located in South Africa; Kiruna (Sweden) and Kourou (French Guiana). The Earth Station situated in Hartebeesthoek, South Africa, is used to confirm the separation of OSTM/Jason 2 from the Delta II. [102]
- **Orbit Acquisition, Assessment and Verification Phases:** From the launch phase to the on-orbit checkout stage, CNES's Satellite Command Control Center (J2CCC) in Toulouse (France) manages satellite control and operations for OSTM/Jason 2. Throughout this duration, the Project Operation Control Center at NOAA in Suitland (Maryland) directs telemetry from two U.S. Earth tracking stations located in Wallops Island and Fairbanks. EUMETSAT transmits telemetry from the Earth tracking station in Usingen to CNES in Toulouse.[102]
- **Initial and Extended Routine Operations Phases:** Routine spacecraft operations transfer from CNES to NOAA's Satellite Operations Control Center (SOOC) in Suitland. The NOAA facility assumes control over the satellite and its instruments, and retrieves mission telemetry data stored by ground stations for the duration of the mission. Meanwhile, the CNES control center maintains surveillance over the satellite, executes navigation tasks, and conducts performance evaluations. [102]

### 2.2 Modes

TTMTTC subsystem was strictly correlated to S/C modes which are briefly outlined below:

- **Satellite Normal Mode:** The Satellite Normal Mode is characterized by the capability to provide generic or specific services such as power management, command execution, status monitoring, precise timing, and fine-pointing capabilities. In this mode, the downlink (TM) rate corresponds to 722.116 kbit/s. Typically, the satellite remains in Normal Mode unless prompted by an alarm or a ground request to transition to a safe or Emergency Mode. [101]
- **Satellite Safe Hold Mode (SHM):** The aim of this mode is to autonomously achieve a safe attitude, in which the satellite provides essential satellite management functions to support vital operations for diagnosis or anomaly handling, including communication between ground and satellite. If this occurs, the down link (TM) rate is decreased to 85.966 kbit/s. Engagement of these modes always occurs in response to a ground request, with transitions consistently initiated from Nominal Mode. [101]

### 2.3 TTMTTC Data Volume

Analysis of literature reveals various methods for distributing data from LEO space crafts. One approach involves setting up continuous return links via GEO relay satellites at data rates of tens of Mb/s. Another method is to arrange direct instrument readouts with continuous broadcasts, dispersing data to ground terminals globally at rates reaching hundreds of kbits/s. Due to the unavailability of data volume for the Jason-2 mission, the value retrieved from the sizing process in subsection 3.6 is considered, with a global value of around 1.2 Gbits in a day. This matches the 2Gbits available on board for payload data storage with an additional 500Mbits for housekeeping.[101] From this, the downlink and uplink data volumes can be distinguished. The space2ground volume represents the majority of the total value; this is expected since it contains both Tracking and Telemetry data, whilst uplink handles the Telecommand alone. The exact computed values are shown in Table 20

### 3 Reverse sizing

The TTMTC subsystem is sized through reverse engineering in order to understand and justify the design choices. The study is carried out on the most demanding scenario in terms of data volume to be transmitted. Regarding the space segment, the sizing is performed for the nominal operating conditions of the mission as both telemetry and scientific data are required to be transmitted to the ground.[68]

The ground segment is sized for the nominal uplink data rate of the mission, assuming a parabolic antenna.[17]

#### 3.1 Antenna Selection

For the space segment, a spiral shaped antenna is chosen as it allows transmission in the S-band with a low output power and high efficiency. Its large beamwidth also eliminates the need of a pointing mechanism for the antenna, saving mass and simplifying the architecture.[96] This choice comes from the heritage of the predecessors of the Jason-2 mission that were already using this type of antenna as it is a standard device in the PROTEUS platform. Specifically, a spiral conical shaped antenna was chosen by confronting the information from the Press kit of the Jason-2 mission and the technical drawings of the PROTEUS platform.[68][30]. Regarding the ground segment, since the S/C is in contact with multiple ground stations as presented in subsection 1.3 the choice was made to do the sizing taking into account a parabolic antenna from the Wallops Command and Data Acquisition Station. [109]

A summary of the diameter (D), pointing accuracy ( $\eta$ ), efficiency ( $\mu$ ) and beamwidth ( $\theta$ ) of the antennas is presented hereafter:

Ground Segment				Space Segment			
D <sub>GS</sub> [m]	$\eta_{GS}$ [deg]	$\mu_{GS}$ [-]	$\theta_{GS}$ [deg]	D <sub>s/c</sub> [m]	$\eta_{s/c}$ [deg]	$\mu_{s/c}$ [-]	$\theta_{s/c}$ [deg]
18	0.01	0.55	0.49	0.19	0.1	0.75	50.53

Table 13: Antenna characteristics

The value of the pointing accuracy of the ground station antenna is taken equal to the pointing accuracy of the DSN while for the space segment the value is taken from literature. [96] Finally, the values of the antenna efficiency were taken from literature.[50][96]

#### 3.2 Frequency Selection, Datarate, and Band

Communication is achieved through the S-band radio bandwidth for both the uplink and downlink channels. A data-rate of 4 kbps and 722.116 kbps are used respectively.[83]. Moreover, the carrier frequency for the downlink is f = 2.21592 GHz and f = 2.04049 GHz for the uplink. [100]

The computed gains values for the receiver and the transmitter antenna in case of downlink and uplink are reported in Table 14.

Uplink f = 2.04 GHz		Downlink f = 2.22 GHz	
G <sub>Rx,s/c</sub>	G <sub>Tx,GS</sub>	G <sub>Rx,GS</sub>	G <sub>Tx,s/c</sub>
49.10 [dB]	10.92 [dB]	49.82 [dB]	11.64 [dB]

Table 14: Antenna gains

#### 3.3 Losses

Only four losses contributions have been considered in the sizing:

- **Free space losses:** occur due to the propagation in space. The largest distance between S/C and GS was considered to be equal to 1336 km, by assuming the orbit to be circular.[17]
- **Atmospheric losses:** caused by the interaction of the signal with gases in the atmosphere. Values are retrieved from literature by taking the frequencies of the carrier in both uplink and downlink modes.
- **Pointing losses:** caused by the offset pointing between the transmitter and receiver. The pointing accuracies are the ones from Table 13.
- **Cables:** Intrinsic property of the cables. The worst case scenario of 3 dB was taken for the sizing.

Rain losses were not taken into account, being negligible in the operating S-band.[50]

The results are summarized in Table 15.

	L <sub>space</sub> [dB]	L <sub>pointing</sub> [dB]	L <sub>atm</sub> [dB]	L <sub>cables</sub> [dB]
Uplink	-161.15	$-4.70 \cdot 10^{-5}$	$-5.00 \cdot 10^{-2}$	-3
Downlink	-161.87	$-5.00 \cdot 10^{-3}$	$-5.00 \cdot 10^{-2}$	

Table 15: Losses

## 3.4 Signal Manipulation

### Encoding

Encoding is a strategy applied to protect the data string from possible errors.

Convolutional encoding, which has a very low error rate, is the one applied for both the uplink and downlink.[17] As no information about the BER was available, typical values of  $\text{BER} = 10^{-5}$  (downlink) and  $\text{BER} = 10^{-7}$  (uplink) were assumed for the sizing. The value of the BER in the uplink case is higher because errors in the uplink may jeopardize the correct positioning of Jason-2's altimeter.[41]

Once the BER and the encoding logic are defined, hypothesizing that the specific logic consists of "Convolutional K = 7 and rate =  $\frac{1}{2}$ ", the minimum energy per bit to noise power ratio ( $\frac{E_b}{N_0}$ ) is retrieved from literature.[50] At the end of the sizing, the computed  $\frac{E_b}{N_0}$  is compared to the minimum one plus an additional 3 dB to grant that the receiver is capable of distinguishing the incoming signal from the noise.

	<b>BER</b>	$(\frac{E_b}{N_0})_{\min}$
<b>Uplink</b>	$10^{-7}$	5
<b>Downlink</b>	$10^{-5}$	4.5

Table 16: Encoding parameters

### Modulation

To transmit over long distances without attenuation, a modulation of the signal is needed. The modulation technique chosen for the downlink is QPSK which optimises the signal's spectrum, allowing to decrease the enlarged data rate coming from the encoding.[108] On the other hand, the uplink uses BSPK for modulation.[108]

	<b>Modulation Technique</b>	$\alpha_{enc}$	$\alpha_{mod}$
<b>Uplink</b>	BSPK	2	1
<b>Downlink</b>	QPSK	2	2

Table 17: Modulation parameters [50]

### Amplification

The amplifier is necessary to give the required power to the signal for the transmission.

The choice of the amplifier is related to the output power required by the signal. This value can be obtained from the literature as a function of the diameter of the ground station antenna and the data rate as shown in Figure 9.[50] Thus a SSA is chosen as the output power is in the typical range of those amplifiers (5W-10W), so the transmitted power ( $P_{Tx}$ ) for the downlink is found.

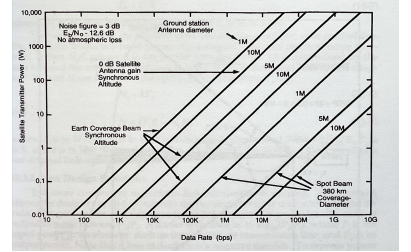


Figure 9: Downlink.

## 3.5 Link Budget

The computation of the total link budget is carried out with the losses, the gains, and the data rate which change depending on the scenario analyzed. Moreover, the Noise ( $N_0$ ) is calculated with the Boltzmann's constant ( $k_b$ ), while two different temperatures are assumed. For the space segment a temperature of  $T = 273$  K is considered due to the reflection of the Sun's rays and the radiation coming from Earth. For the ground segment  $T = 293$  K was selected as the antenna is exposed to the ambient temperature.[109] The bandwidth (B) is chosen to be 30 MHz, as it is a typical value taken for a conservative sizing.

The  $P_{Tx}$  for the uplink was retrieved from the datasheet of an S-band antenna in the Wallops Command and Data Acquisition Station [66]. The losses, the  $P_{Tx}$  and the  $G_{Tx}$  are used to compute the receiver's power ( $P_{Rx}$ ), from which the Carrier Modulation Index Reduction ( $P_{mod,loss}$ ) is subtracted. As no value of  $\beta_{mod}$  was found,  $\beta_{mod}$  was assumed to be  $78^\circ$  being a typical value. The energy per bit over noise density and the signal to noise ratio for both uplink and downlink are shown in Table 18.

	<b>P<sub>Tx</sub> [W]</b>	<b>P<sub>Rx</sub> [W]</b>	<b>EIRP [dB]</b>	$\frac{E_b}{N_0}$ [dB]	<b>SNR [dB]</b>
<b>Uplink</b>	300	-79.31	32.69	85.59	36.21
<b>Downlink</b>	10	-96.42	18.64	49.24	19.41

Table 18: Link budget and Signal to Noise Ratio

These results confirm that the minimum threshold for the  $\frac{E_b}{N_0}$  is satisfied.

The same result is obtained for the SNR, as the  $SNR_{min}$  is set at 10 dB, as it is the most conservative value being related to the DSN which is the most powerful transmitting network.[64] The condition to achieve a correct tracking and distinction of the signal is satisfied, as the difference between SNR and  $SNR_{min}$  is higher than 3 dB.

### 3.6 Ground Station Selection

The ground station selection is fully dependant on the orbital parameters of the nominal orbit of Jason-2 as the orbit is constrained due to the scientific requirements. The vital parameters that affect the choice of the GS are the latitude, longitude, allowable elevation, and azimuth angles. This is because determine the possible field of view of the station and its contact time with the satellite, which is of paramount importance given the constraint on the altimeter's measurements that are required to be transmitted in near real time.[82][10] Thus, the choice of multiple GSs that allow a complete coverage of the satellite's ground track is the optimal solution.[17]

#### Contact Strategy

In order to compute the contact window, the visibility window needs to be calculated first. The visibility window is the time duration when the satellite passes in the field of view of the ground station antenna, which is taken equal to the beamwidth of the ground station antenna. Its value is  $50.54^\circ$  and is taken using the characteristics of the ground antenna in subsection 3.2.

The orbit is assumed to be circular, with an altitude of  $r_{SC}$ . The arc of contact can be derived from trigonometry and then Kepler's Law is applied in order to compute the contact time.[14]

Arc of contact	Visibility window	Real visibility window
43.10 deg	13 min	9 min

Table 19: Visibility window

The actual visibility time window is obtained by accounting for the time to lock in, unlock and correctly point the ground station; it was assumed to be 4 min overall.[50] The contact window is obviously constrained by the visibility window, and the maximum contact window duration is 9 minutes.

The entity of the data nominally transmitted to the ground is computed by inverting the definition of the data rate, knowing that the given value of the downlink is averaged on the day. The hypothesis of three successful passages above the GS over one full day was made. This assumption comes from the fact that NOAA provides two of its stations at Wallops Island, VA, and at Poker Flats, AK while EUMETSAT provides its station in Usingen, Germany. [17]

This leads to a data volume in the worst case scenario, i.e. if respectively only downlink or uplink communication is achieved during the contact window.

	Downlink	Uplink
Maximum Data Volume [Mbits]	1170	6.48

Table 20: Maximum data volume exchanged

The results are compliant with the typical contact times and data rate for LEO satellites, confirming the effectiveness and productiveness of scientific missions in LEO.[82][34] Moreover, as already mentioned, the data storage available for payload is 2 Gbits with an additional 500 Mbits for housekeeping [100].

### 3.7 Antenna Positioning

To allow for a correct pointing of the antenna, the optimal solution is to place them on the Nadir-pointing surface of the satellite. In this way, no DOFs are added and the pointing driver of the mission can be exploited. For redundancy reasons, the number of antennae shall be greater than one in order to account for possible failures of the ADCS; or, in the event of a safe mode, to communicate with the GS even if the Nadir-pointing condition is not satisfied.

### 3.8 TTMTTC Budget

The mass and power budget for the space segment are presented in Table 21. For the antennae, the sized values have been used and the number of antennae is taken as two for redundancy.[18] The input power for the antenna is deduced from literature knowing the output power and amplifier.[50] Furthermore, all the payloads that independently transmit data to their dedicated ground stations have been included.[17] [3]

	Spiral Conical Antenna	DORIS	LRA	GPSP
Mass [kg]	1	1.5	2.2	10
Power [W]	50	30	0	17.5

Table 21: TTMTTC mass and power breakdown

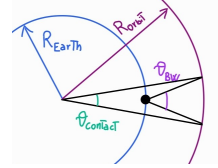


Figure 10: Contact window.

## **Homework 4**

### **Attitude Determination & Control Subsystem**

# 1 AOCS Architecture

As part of the multi-mission platform PROTEUS family, Jason-2 shares the AOCS system strategy with other missions; however, specific adaptations were applied to suit its goal: serving as a low orbit satellite for high precision Earth Observation. The satellite must meet two requirements: maintain a fixed nadir (Earth-pointing) orientation for the altimeter boresight and align solar arrays with the Sun.[113] This dual orientation ensures continuous altimeter measurements of the ocean surface while optimizing the satellite's power supply. Achieving this balance relies on on-board calculations performed by the AOCS, leveraging data from attitude sensors and various catalogue and models (magnetic fields, star catalogue, etc.).[100] An overview of this subsystem is shown in Figure 11. The functional redundancies are fully ensured at satellite level, so that the equipment units are either one-to-one or "n" out-of "m" redundant (e.g. 2 gyros out of 3).[36] Orbit determination is carried out by the on-board payload (DORIS, GPSP, LRA) as part of the tracking system and it is therefore not analysed in this report.

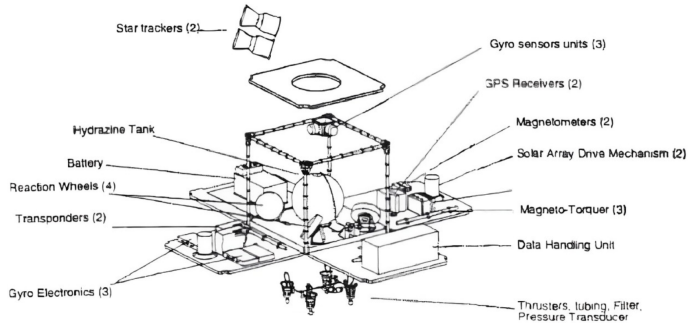


Figure 11: Proteus overview

## 1.1 Attitude Determination

### 1.1.1 Sensors

To determine its orientation accurately at any given moment, Jason-2 relies on a combination of two star trackers and three onboard gyroscopes. Additionally, orientation can be established using eight coarse sun sensors and a three-axis magnetometer. An overview of the sensors along with their configurations are presented below.[92]

**Star Trackers (STR):** the spacecraft uses one of two three-axis CALTRAC Star Trackers placed in a redundant configuration (one is nominal and the other one is redundant) with an accuracy of 15 arc-sec ( $3\sigma$ ). These sensors can observe stars of magnitude 4.3 or brighter and have a field of view of  $22^\circ \times 18^\circ$ , which reduces star gaps and provides better knowledge resolution on the tracker boresight. The Star Trackers are accommodated on the payload in a Star Tracker Assembly (STA) equipped with an autonomous thermal control.

**Gyroscopes (GYR):** 3 two-axis gyros are employed, two of the three are nominal whilst the third one is redundant; this approach was selected due to the significant utilization across the PROTEUS control modes. Gyros are mounted in an orthogonal configuration on the spacecraft, thus providing redundant measurements on the three orthogonal spacecraft axis. Gyros are the baseline error sensors for all modes except for the survival mode.

**Magnetometers (MAG):** the attitude sensor system is composed by a three-axis Magnetometer with an analog output and a sensitivity lower than 4 mgauss. This component provides redundant measurements of the local Earth magnetic field which are used during the mission to provide momentum management control signals. To ensure proper data acquisition, MTBs are not commanded during measurements.

**Coarse Sun Sensors (CSS):** The CSS consists of eight analog solar cells mounted on Jason-2 to provide 4-pi steradian coverage in a non-redundant implementation with an accuracy of  $3^\circ$  plus albedo. Pitch and Yaw axes sun sensors each use four cells.

### 1.1.2 Attitude Determination Algorithm

By taking advantage of the multi-sensor's information, the attitude determination can be completed with higher accuracy and malfunction tolerance capacity than with a single sensor. Nevertheless, the characteristic of onboard sensors differ greatly.[62] For instance, the gyro have excellent performance for short periods, whereas in the long term the accuracy becomes unacceptable. On the other hand, star trackers are known to be the best attitude sensor; however, they have much lower update rates and they can be interrupted by sunlight, and reflective light from Earth.[62]

Following these considerations, Jason-2 relies on a gyro-stellar hybridization in which gyros are used for short term attitude measurements, and the star tracker measurements are used to compensate for the gyros drift error effect.[36] This process is done through an on-board Kalman filter: a classical recursive filter that uses the measurements of a system and a mathematical model of its dynamics to estimate the its state. This is particularly useful for systems that are subject to noise and uncertainties.[91] This control algorithm is based on quaternion feedback; the attitude representation of choice for most Kalman filtering applications.[92, 91]

## 1.2 Attitude and Orbit Control

### 1.2.1 Actuators

The selected actuators for attitude control are reaction wheels and magneto torquer bars; on the other hand, for orbit control, thrusters are employed.

**Magnetic Torquer Bars (MTB):** MTB with redundant coils are employed to counteract RW saturation caused by the accumulation of angular momentum. This momentum dumping technique provides a cheap and reliable solution that takes advantage of the Earth's magnetic field and it is therefore ideal for LEO satellites like Jason-2.[16] MTB are sized for SHM which requires more torque than the momentum management application.

**Reaction Wheels (RW):** Jason-2 makes use of four RW to generate torque for attitude command. These momentum exchange devices are Teldix' RSI 8-120/351 and produce a torque of 0.1Nm (worst case) on each axis for a maximum duration of around 1 minute.[36, 100] RW are commonly used in small-medium spacecrafts like Jason-2 since they are ideal for precise pointing with lower values of torques. Additionally, they only require electrical power that can be supplied by the solar panels. Full three axis control requires 3 RW; however, having 4 is the best option for redundancy reasons.[33] For Jason-2, a pyramid configuration (Figure 12) was chosen. This is the most common configuration for Earth-pointing spacecraft in which a constant pitch rate is required to point the instruments towards the earth surface. [23] The 4 RW operate simultaneously to avoid attitude errors due to wheel zero-speed crossing; this problem would occur with only 3. RW are also one of the main sources of attitude disturbances; this was minimised by locating the wheel close to the centre of mass of the satellite.

**Thrusters (THR):** Four thrusters are located and oriented as shown in Figure 12. These thrusters are used to provide  $\Delta V$  actuation in either four thrusters mode or two thrusters mode. Four thrusters are only used early in the mission for large  $\Delta V$  maneuvers ranging from meters to tens of meters per second. Minor adjustments, ranging from centimeters down to millimeters per second, are performed with only two thrusters.

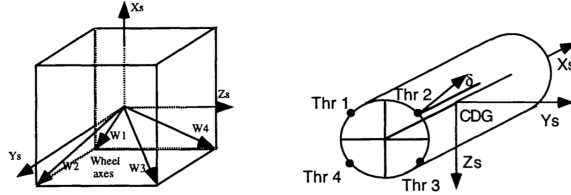


Figure 12: RW and thrusters configuration

### 1.2.2 Attitude Control Algorithm

To maintain a solar pointing orientation of the solar array cell side and simultaneously a nadir orientation of the altimeter antenna boresight, a yaw steering and solar array pitch algorithm for the three-axis stabilized spacecraft were required [114]. As shown in Figure 13, this implies a rotation around the yaw axis of the spacecraft, which in combination with an independent pitch-axis rotation of the solar arrays, grants orthogonality between the cell surface and the sun rays. The yaw steering of the spacecraft and the rotation of the solar arrays is mainly based on two parameters:  $\beta'$  which is the angle between the orbital plane and the Earth-Sun vector, and  $\nu$  that is the angle between the Earth-Sun vector projected onto the orbital plane and the Earth-satellite vector. The algorithm consists of five yaw modes, each corresponding to a certain  $\beta'$  range as shown in Figure 14.

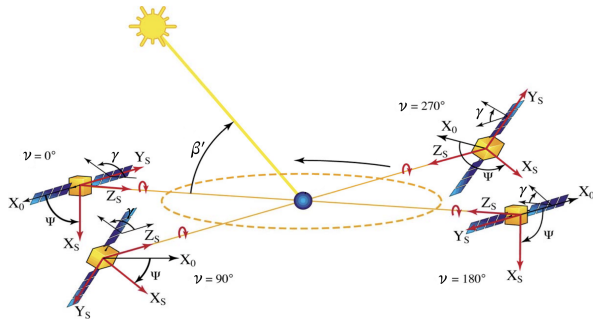


Figure 13: Yaw steering and solar array pitch [100]

Yaw Steering Algorithm		
Yaw Regime	Occurrence	Description
Sinusoidal	$ \beta'  > 15^\circ$	Yaw sinusoidal law
Fixed	$ \beta'  < 15^\circ$	Yaw = $0^\circ$ if $\beta' > 0^\circ$ Yaw = $180^\circ$ if $\beta' < 0^\circ$
Ramp-up	$ \beta'  \geq 15^\circ$	Yaw fixed to sinusoidal
Ramp-down	$ \beta'  \leq 15^\circ$	Yaw sinusoidal to fixed
Yaw flip	$ \beta'  \approx 15^\circ$	Yaw = $0^\circ$ if $\beta' > 0^\circ$ Yaw = $180^\circ$ if $\beta' < 0^\circ$

Solar Array Pitching Algorithm		
Pitch Angle	Occurrence	Description
$\gamma = 90^\circ + \nu$	$0^\circ < \beta' < 15^\circ$	Fixed yaw (flying forward)
$\gamma = 90^\circ - \nu$	$-15^\circ < \beta' < 0^\circ$	Fixed yaw (flying backward)

$\gamma = \arctan \left( \frac{\sin(\nu + 90^\circ)\cos\beta'}{\cos(\nu + 90^\circ)\cos\beta'\cos\nu - \sin\beta'\sin\nu} \right)$	$ \beta'  \geq 15^\circ$	Sinusoidal yaw + transition regimes
------------------------------------------------------------------------------------------------------------------------------------	--------------------------	-------------------------------------

Figure 14: Attitude control algorithms [114]

## 2 Operational Modes

PROTEUS has five distinct operational modes which are specific to various stages of the mission, each employing a designated subset of hardware to meet performance goals. Each mode is provided with a concise functional overview, detailing the attitude determination and control algorithms utilized.

### SHM - Safe Hold Mode

SHM activates upon detecting anomalies or hardware failures and during the initial attitude acquisition post-launch separation. It aligns the spacecraft's -X axis with the Sunline and damps inertial rates to enable solar array power generation and establish an initial attitude reference. Relying on simple and reliable sensors and actuators — such as a 3-axis magnetometer and 8 Coarse Sun Sensors for rough attitude rate estimation and sun direction determination, and 3 Magnetotorquer bars and 2 of 4 reaction wheels for kinetic momentum — the SHM control laws first damp the inertial body rates using MTB as magnetic brakes to dissipate any initial kinetic energy of the body. Maintaining spacecraft alignment with the Sunline is achieved through gyroscopic stiffness generated by constant-speed rotation of the reaction wheels, ensuring stability against environmental torque disturbances.[92, 81]

### STAM - Star Acquisition Mode

The objective of STAM is to acquire stars in the STR and enhance both attitude determination and control to initiate the Normal Operation Mode effectively. Initially, the spacecraft is positioned approximately on the Sunline with moderate attitude and attitude rate errors. The process begins by commanding the wheels to dampen spacecraft rates using gyroscopic data. Attitude knowledge is then initialized by leveraging measurements from the Sun and magnetic field vectors obtained through the MAG and CSS systems. Subsequent measurement are collected and processed over a period of time by a Kalman filter in order to improve the knowledge of attitude and body rate. Once attitude determination reaches a sufficient precision, the spacecraft is commanded to slew to a predetermined acquisition guide star field. Visible stars in the STR field of view are downlinked to the ground for confirmation before being integrated into the Kalman-filtered attitude solution. Once the filter sufficiently converges on the star vectors, the ground is able to command the transition to Normal Operation Mode.[92, 81]

### NOM - Nominal Operation Mode

NOM represents the operational mode for executing all scientific missions. Target attitude is provided from ground employing either harmonical or polynomial profiles for angular rates. Spacecraft stabilization relies on four canted Reaction wheels, with a backup capacity of three wheels. Using these Reaction wheels, the spacecraft achieves inertial stabilization, while Kalman filtering of STR and GYR data maintains attitude knowledge at the arc-second level. Attitude control is executed by dispatching a sequence of time-tagged quaternion commands to the control law, effectively aligning spacecraft attitude with the current command. To orient towards an inertially fixed target, the quaternion command remains constant, whereas for Earth-relative pointing, the quaternion command evolves over time. Throughout NOM operations, any surplus momentum accumulated in the reaction wheels due to external torque disturbances is dissipated magnetically using the MTB.[92, 81]

### OCM - Orbit Control Modes with 2 or 4 Thrusters

Maneuvering is provided by four 1 N thrusters with double seats and double valves, alongside 28 kg of hydrazine stored in a membrane tank operated in blowdown mode. These thrusters are canted to enable three-axis control via modulation commands. OCM4 serves to execute significant  $\Delta V$  adjustments. During this mode, thrusters handle both propulsion and attitude control, with the wheels remaining inactive. The standard operating procedure for four thrusters entails continuous firing until any deviation in attitude is detected, prompting off-pulsing of the thrusters to generate a corrective torque. OCM2 is designated for fine  $\Delta V$ . In this mode, two thrusters operate continuously while reaction wheels maintain attitude. Attitude determination continues to rely on the STR/GYR Kalman filter.[92, 81]

	GYR	STR	CSS	MAG	RW	MTB	THR
Safe Hold Mode ( <b>SHM</b> )	0	0	8	1	2	3	0
Star Acquisition Mode ( <b>STAM</b> )	2	1	8	1	4	3	0
Normal Operation Mode ( <b>NOM</b> )	2	1	0	0	4	3	0
Orbit Control Mode 2 thrusters ( <b>OCM2</b> )	2	1	0	0	0	3	2
Orbit Control Mode 4 thrusters ( <b>OCM4</b> )	2	1	0	0	4	3	4

Figure 15: Operational modes

### 3 AOCS Pointing Budget

Hereby the pointing budget is presented. It was necessary to uphold attitude knowledge to a precision of less than  $0.05^\circ$  and attitude control to within  $0.1^\circ$  at  $3\sigma$  for each axis during standard operations.[100][26] Moreover, no constraint on the rates is considered for the pointing budget. More specific requirements regarding each control modes, particularly referring to P/Ls, TCS and TTMTTC subsystems are indicated in Table 22. The most constraining values are associated to the payloads as the mission requires an high accuracy pointing, so a higher knowledge accuracy is mandatory in order to satisfy the scientific requirements. These values are enforced during the whole mission, except during the Launch and Early orbit phase, the Orbit Acquisition phase and SHM where the priority is shifted to the monitoring of the satellite.

The same logic can be applied to the TTMTTC subsystem, where the antenna is cantilevered on the same face as the one of the payloads performing Nadir-pointing. However, during the orbit changes and safe mode, a lower APE is required in order to ensure that communication with ground is kept.

On the other hand, as the temperature gradients that the satellite needs to withstand throughout the mission are not critical, a more relaxed pointing budget is defined for the TCS. Most values are taken as general reference for reverse sizing due to the lack of literature references. N/A denotes that the subsystem has no influence on the pointing budget in that specific mode.

	SHM	STAM	NOM	OCM
P/L	N/A	APE < $0.15^\circ$ AKE < $0.05^\circ$	APE < $0.15^\circ$ AKE < $0.05^\circ$	N/A
TCS	APE < $0.15^\circ$	APE < $0.15^\circ$	APE < $0.5^\circ$	APE < $0.1^\circ$
TTMTTC	APE < $0.05^\circ$	N/A	APE < $0.15^\circ$	APE < $0.1^\circ$

Table 22: Pointing Budget

For the EPS the most critical pointing constraints are during detumbling and the SHM as energy needs to be provided to the whole space segment. However, when compared to the subsystems in Table 22 the EPS requirements are less significant.

### 4 Reverse Sizing

In order to size the ADCS, once the pointing budget per each mode was defined, it was possible to select the best suite of sensors and actuators to achieve the required accuracy. Then, calculating the disturbing torques allowed for consideration on the desaturation mechanism and slew maneuvers. Lastly, the subsystem's mass and power budgets are detailed.

#### 4.1 Attitude Sensor Suite Selection

The selection of the sensors is based on the AKE that shall be granted throughout the modes of the mission. The sensors that better achieve the requested AKE, and therefore APE, described in Table 22 are star sensors.[50] Their high accuracy and ability to provide full attitude determination make them extremely valuable, also being prone to failure a cold redundancy is implemented. However, their high power consumption prompts a cheaper alternative in SHM using 8 sun-sensors prioritizing energy efficiency over pointing precision. Sun sensors are also preferred in STAM to prevent star sensors damage.

Since Jason-2's orbit is strongly affected by the presence of the magnetic field, magnetometers can be considered for aiding in the computation of the attitude and the estimation of the local magnetic field to support the magneto-torquers.[80] However, MAGs alone cannot fully determine attitude since they provide partial determination by measuring only one vector. Additionally, it should be noted that neither MAGs nor CSS meet the accuracy requirements of the Star sensors. [50] For this reason, they shall be used only in non-nominal modes in case of failure of Star sensors. Coupled with these sensors, gyroscopes can be implemented for orbit determination and, with a correct attitude kinematic model, attitude determination as well. However, they're not used in SHM due to the high power consumption

#### 4.2 Attitude Actuator Suite Selection

A three-axis control strategy has been selected to stabilize Jason-2 satellite. In accordance to Table 22, a combination of reaction wheels and magnetotorquer bars are selected as actuators. This selection ensures the attainment of the required APE throughout the entire mission duration while maintaining stable pointing. Given that RW offer axial control, a redundant pyramidal configuration of four wheels is implemented to mitigate disturbances and stabilize the satellite during detumbling and slew maneuvers. This configuration allows to cope with possible failures as a hot redundancy is implemented.[23] However, due to their considerable energy

consumption, only two wheels are utilized in SHM to prioritize energy efficiency. The presence of reaction wheels requires the use of MTB for desaturation and additional momentum dumping. Given that Jason-2 operates in a LEO characterized by a significant presence of Earth's magnetic field, MTBs are highly suitable. Three of them are always used providing three-axis stabilization and presenting a energy-efficient and reliable solution. A set of 4 thrusters is also employed exclusively for orbit control.

### 4.3 Disturbances Effects

The perturbations that affect the Jason-2 mission throughout its phases and modes are:

- Gravity Gradient:** It is caused by a non-uniformity in the gravitational field. The entity of the disturbance was estimated starting from the definition of the inertia matrix of the spacecraft, which was obtained, in first approximation, from the value of the total mass of the satellite and its dimensions, also taking into account the deployed solar arrays on the roll axis.[68]

The parameters used to compute  $T_{GG}$  are reported in Table 23. Moreover, the maximum deviation of the pitch axis from the local vertical ( $\theta$ ) was assumed  $45^\circ$  to obtain the most conservative value of  $T_{GG}$ . R is found by approximating the orbit as a circular one, having a low eccentricity.[69] The maximum and minimum values of the inertia moments were extracted from the inertia matrix obtained in body coordinates.

$I_{\max} [kg \cdot m^2]$	$I_{\min} [kg \cdot m^2]$	R [km]
881.8	303.8	7714

Table 23:  $T_{GG}$  parameters

- Solar Radiation Pressure:** The solar radiation that illuminates the surfaces of the spacecraft generates a pressure which is unbalanced with respect to the centre of mass of the satellite, that in turn cases a disturbing torque.[23] Due to the uncertainty in the location of the centre of mass of the spacecraft ( $C_g$ ) the difference between the two centres is assumed 3 cm as a conservative value. For the same reason, the incidence angle ( $I$ ) is assumed equal to  $0^\circ$ .[50]  $A_s$  is taken as the cross section of the S/C and the area of the two solar panels. This is the worst case scenario because in this case the exposed area is maximum. The value of the reflectivity coefficient  $q$  is taken as the typical conservative value. [56]

$F_s [W/m^2]$	$A_s [m^2]$	$q [-]$	$C_{mis} [cm]$
1975	10.8	0.6	3.0

Table 24:  $T_{SRP}$  parameters

The value of the solar contribution  $F_s$  is defined as a summation of contributions from the direct solar radiation at 1 AU, the radiation and the albedo coming from Earth at the orbit's altitude.[23]

- Magnetic Torque:** It is generated due to the presence of the residual magnetic induction ( $m$ ), as a consequence of parasitic currents. The residual dipole is estimated from literature by assuming Jason-2 as a Class II spacecraft. [15] The magnitude of the magnetic field ( $B$ ) was computed by approximating it to a dipole. This approximation is acceptable for a preliminary analysis, however, for a more accurate estimation, the spherical harmonics can be implemented. Finally, M is the Earth magnetic moment.

$B [T]$	$m [A \cdot m^2/kg]$	$M [Tm^3]$
$3.47 \cdot 10^{-5}$	$3.5 \cdot 10^{-3}$	$7.96 \cdot 10^{15}$

Table 25:  $T_{mag}$  parameters

- Air Drag:** The drag perturbation is the effect from the interaction between the satellite and the residual atmosphere which generates aerodynamic forces.[23] The misalignment  $C_{mis}$  between the centre of pressure ( $C_{ap}$ ) and the centre of mass is evaluated as in the SRP case. Additionally, the drag coefficient ( $C_d$ ) is taken as the typical value for a LEO orbit. [56]

The density of the atmosphere  $\rho$  at the altitude of Jason-2 orbit is estimated from the Exponential Atmospheric Density model.[104] Finally, the relative velocity  $v_{rel}$  is computed as the difference between the orbital speed of the satellite and the tangential velocity of the Earth, assuming that the atmosphere moves rigidly with the planet. [23]

$\rho [kg/m^3]$	$C_d [-]$	$A [m^2]$	$v_{rel} [m/s]$	$C_{mis} [cm]$
$3.09 \cdot 10^{-15}$	2.5	3.7	$6.626 \cdot 10^3$	3.0

Table 26:  $T_{drag}$  parameters

### 4.3.1 Perturbing Torques

In table Table 27 the results of the previous analysis are summarized. The perturbations are classified with **constant** or **cyclic** based on the type of pointing that Jason-2 performs throughout the mission, which is Nadir-Pointing.

	$\mathbf{T}_{GG} [Nm]$	$\mathbf{T}_{mag} [Nm]$	$\mathbf{T}_{SRP} [Nm]$	$\mathbf{T}_{drag} [Nm]$
Magnitude	$7.526 \cdot 10^{-4}$	$6.935 \cdot 10^{-4}$	$3.415 \cdot 10^{-6}$	$1.839 \cdot 10^{-8}$
Type	Constant	Cyclic	Cyclic	Constant

Table 27: Estimation of perturbations

The total torque is computed as the sum of all the contributions and a 100% margin is added to this value, leading to  $T_{tot} = 0.0016 Nm$ . The greatest disturbing torques are the Gravity Gradient and Magnetic Torques as expected from a non sun-synchronous LEO orbit.[23]

## 4.4 Attitude Actuators Sizing

Due to the lack of exact information in the literature on the technical values of chosen actuators for the Jason-2 mission, the data from the RSI 12-75/60 model was used for conservative reasons, as it is a previous version of the actual reaction wheels used in the Jason-2 mission.[58] The maximum angular momentum is therefore set to  $\mathbf{H}_{max} = 12 \text{ Nms}$  and the maximum torque to  $\mathbf{T}_{max} = 0.075 \text{ Nm}$ .

Knowing the maximum angular momentum and torque provided by the RW, the following step of the sizing was to asses the capability of the actuators to counteract the disturbances. The most conservative scenario was analyzed, considering in the computation only a single operating reaction wheel. This prevents saturation of any individual wheel while maintaining functionality of the remaining ones.

### 4.4.1 Desaturation

Firstly, the number of orbits that it takes for the reaction wheels to saturate was evaluated. The maximum storable angular momentum ( $H_{max-stored}$ ) was calculated from the total torque found in subsection 4.3 and the period of one orbit. The analysis yields that the reaction wheel reaches saturation every orbit. From this result, the desaturation mechanism was sized.

The desaturation is performed with magneto-torquers as it is possible to exploit the presence of the magnetic field, moreover the advantage of using such actuators is that they are energy efficient, reliable and use no fuel which is a important resource for the orbit maintenance of the Jason-2 mission. Thus the thrusters are used only for station keeping manoeuvres and not for the desaturation.[68]

The value of the dipole of the magneto-torquers ( $D_{magn}$ ) was assumed from the literature of the PROTEUS platform which stated the dipole entity in nominal operating conditions.[100] Consequently, the time that the magneto-torquers takes ( $t_{desat}$ ) to desaturate one reaction wheel was computed from the available dipole, the angular momentum of the reaction wheel to be desaturated and the value of the magnetic field. The result showed that the desaturation lasts for 2.57 orbits, due to the fact that only during the SHM the magneto-torquers can provide up to  $180 Am^2$  when the payloads are switched off, which is higher with respect to the nominal one.

$H_{max-stored} [\text{Nms}]$	$D_{magn} [Am^2]$	$t_{desat} [h]$
11.1	20	4.81

Table 28: Desaturation of one reaction wheel

### 4.4.2 Slew Manoeuvres

A Slew Manoeuvre represents a controlled motion between two attitudes.[23] In the Jason-2 mission, once the nominal orbit is reached, a Slew Manoeuvre is hypothesized to be executed in order to set the satellite in NOM. Since the entity of the slew angle to be performed is unknown, a worst case scenario is assumed where the slew angle is  $180^\circ$ . The same entity is assumed when Jason-2 has to pass to the SHM. On the other hand, during the OCM the attitude motion is not performed by the RW, but by the magneto-torquers, which operate with a dipole of  $20 A \cdot m^2$  in nominal conditions. Thus, to size this manoeuvre the same conditions as the previous one are assumed due to the lack of data and for a conservative sizing. Furthermore, it is hypothesized that the acceleration given by the actuators is constant and that the coasting phase can be neglected.[50] Adding to those considerations, the slew rate of the manoeuvre was assumed to be  $0.5^\circ/s$  which is a typical admissible value for payloads.[50]

From the computations, the torque required to perform such manoeuvre at the assumed slew rate could not be provided nor by one reaction wheel, nor by the magneto-torquers. Thus, it was chosen to impose the

admissible torque level ( $T$ ) and compute the time ( $t_m$ ) and slew rate necessary ( $\dot{\theta}_m$ ) to carry out the manoeuvre with a slew angle ( $\theta_m$ ) of  $180^\circ$ .

Slew Manoeuvre	$\theta_m$ [°]	$\dot{\theta}_m$ [°/s]	$t_m$ [s]	$T$ [Nm]
Reaction Wheel	180	0.468	384	0.075
Magneto-torquer	180	0.045	4000	$6.935 \cdot 10^{-4}$

Table 29: Slew Manoeuvres

The results showed that in the case of the slew manoeuvres performed by a single reaction wheel, a minor increase in the maneuvering time and a decrease in the slew rate are necessary to meet the mentioned constraints. On the other hand, for the slew manoeuvre to orient the spacecraft for the OCM, the time required saw a great increase due to the low dipole provided by the magneto-torquers. In any case, the achieved slew rates and time of the maneuvers were acceptable in the context of the mission as both slew rates are kept under the assumed maximum slew of  $0.5^\circ/\text{s}$  and the time required is kept under one orbital period.

## 4.5 Fuel Mass Sizing

As attitude control, desaturation and slew maneuvers rely solely on reaction wheels and magnetotorquer bars, no fuel mass needs to be sized for these purposes. The onboard thrusters are exclusively utilized for orbit control. This decision stems from the inability of these thrusters to achieve the necessary APE for the payloads.[50]

## 4.6 Positioning of Sensors and Actuators

In assessing the setup of sensors and actuators, both their characteristics and failure modes are considered. To protect their optics, Star sensors would be mounted on the side opposite to the Nadir-pointing surface, facing deep space for optimal data acquisition.[23] At the same time, coarse sun sensors would be mounted on each satellite face to determine Sun's position and control the opening or closing of the optical protections for the star sensors. Magnetometers shall be mounted away from electronics to prevent any interference with magnetic field data. A set of three orthogonal sensors has to be implemented to determine the magnetic field vector in body frame.[80]. Gyroscopes are installed in an orthogonal arrangement on the spacecraft, ensuring redundant measurements along all three spacecraft axes. Regarding the actuators, the RW pyramidal configuration allows each wheel to have a component of the torque along all three axes, mitigating errors due to zero-speed crossing. Moreover, a square based pyramid configuration could best suite the geometry of the PROTEUS platform which has an nearly perfect square base.[100] A configuration identical to MAGs is adopted for MTBs to ensure that no unwanted magnetic field is induced in the spires, ensuring accurate torque provision.

## 4.7 Subsystem Budgets

The ADCS mass and power budget is reported, all the values are taken from literature. For the former, the mass and the power budget of the single element are reported. Then,in section 2, the power budget is evaluated for the identified modes,as not all the sensors and actuators are active during all modes.

Element	GYR[57]	STR[49]	CSS[99]	MAG[94]	RW[12]	MTB[45]
Mass budget [kg]	0.650	0.235	$0.5 \cdot 10^{-3}$	0.1	4.85	7.8
Power budget [W]	3.75	1	$3.3 \cdot 10^{-4}$	1	45	3.8

Table 30: Mass and power budget for each element

	GYR[57]	STR[49]	CSS[99]	MAG[94]	RW[12]	MTB[45]	Total
<b>SHM</b>	0	0	$2.64 \cdot 10^{-3}$	1	90	11.4	102.4
<b>STAM</b>	7.5	1	$2.64 \cdot 10^{-3}$	1	180	11.4	200.9
<b>NOM</b>	7.5	1	0	0	180	11.4	199.9
<b>OCM2</b>	7.5	1	0	0	0	11.4	19.9
<b>OCM4</b>	7.5	1	0	0	180	11.4	199.9

Table 31: Power Budget per mode [W]

The total mass budget results to be 44.674 kg, this is coherent with the preliminary mass percentage of 9% [55](47.25 kg) allocated for attitude control subsystem. Similarly, the highest power budget required per mode is 200.9 W which aligns with the 19% [55] (110.2 W) of the total power budget considering the applied 100% margin.

# **Homework 5**

## **Thermal Control Subsystem**

# 1 TCS Architecture

The goal of the TCS is to maintain all the elements of a satellite system within their temperature limits for all mission phases, while minimizing the power consumption of the active thermal control.[2] For LEO satellites like Jason-2, the main sources of environmental heating are solar radiation, albedo, and the infrared energy emitted by Earth. The internal heating instead comes from the heat dissipation of components within the spacecraft.[47] As part of the PROTEUS platform family, Jason-2 has a combination of active and passive control elements, with specific adaptations in the radiator sizes and heating parameters.[68]

## 1.1 Passive Control

Passive thermal control acts as heat rejection, insulation from the environment, and thermal decoupling between components. For instance, the PROTEUS platform and the Jason-2 payload are thermally decoupled using four interface titanium alloy pods, in which the remaining thermal conductive coupling can be assumed to be less than  $0.04 \text{ W}/\text{°C}$  for each pod.[100] The passive thermal control is sized to obtain the maximal authorized temperature on the equipment in the hottest cases. The components selected for Jason-2 are showed below.[2]

**Radiators:** In order to dissipate excess heat via radiative heat transfer to the outer space, radiators are used.[63] Jason-2 makes use of silvered second surface mirrors (SSM) on the radiators to improve the heat rejection and at the same time reduce the absorption of external solar fluxes. On top of this, aluminum doublers are added to enlarge the conduction and spread heat in the radiators, and white paint is applied to the cylindrical radiator of the launcher adaptor to insulate from radiation. Battery, propulsion and platform equipment units, all have their own radiator.[84]

**MLI blankets:** Multi Layer Insulation (MLI) are applied both internally and externally of the spacecraft to preserve it from the extreme environment in space and to help thermally isolate the PROTEUS platform and the payload module.[106] MLI consist on thermal insulation composed of multiple layers of optical and electrically conductive materials separated by thin netting spacers; the equivalent efficiency of this blanket is  $0.1 \text{ W}/\text{m}^2/\text{°C}$ .[100] The outer layer of the blanket is made of Kapton, selected because it is a low emittance polyimide film that remains stable across a wide range of temperatures.[68] All the external requirements are covered by MLI, except the ones requiring a field of view with Sun or Earth that are essential for the success of the mission.

**Thermal straps and Insulating Washers:** Thermal straps are applied to ensure conductive coupling between two parts. Contrarily, permaglass thermal insulating washers are used to reduce conduction (e.g. battery zone).

## 1.2 Active Control

The active components for thermal control are the electrical heaters; these are sized with significant margins to meet further worst case conditions.[68, 100, 77] The ATC is sized to withstand the coldest cases and is not foreseen for the launching phase. [2, 100] The active thermal control concept shown in subsubsection 1.2.1 guarantees good performances in terms of thermal stability and precision.

**Electrical Heaters** The Electrical Heaters are a source of heat based on the Joule effect, they work converting electric current into heat. If powered and handled correctly, the active thermal control can give a high level of thermal protection providing ten regulated heating lines for the platform and eleven regulated heater lines for the payload both in a cold redundancy.[106, 100]

### 1.2.1 ATC Algorithm

The ATC heating concept is represented in Figure 16

The heating lines are managed in a closed-loop system using a PI algorithm, which is operated by a regulation algorithm running on the On Board Software. [100]

The standard thermal control operates in a cyclical process at a frequency of  $1/32 \text{ Hz}$  with a command resolution of 1 second. During each cycle, the active thermal control loop retrieves measurements from three thermistors, calculates the median temperature value, and subsequently determines the power injection command. This command is derived by evaluating the temperature error and applying PI correction. Both the temperature error and the power injection command are then memorized for utilization in the subsequent cycle.

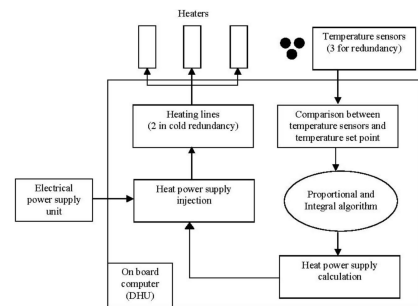


Figure 16: ATC algorithm [106]

Furthermore, the power injection command computation algorithm is initialized for each control loop.

While this approach indeed demonstrates excellent thermal stability and precision, its selection primarily arises from the necessity for adaptability and flexibility. These requirements are crucial not only during the developmental stages but also throughout the flight via command uploads. [106]

## 2 Thermal control description and rationale

The thermal control system of the PROTEUS platform is divided into five distinct parts, each designed to be as uncoupled as possible from the others [2] [106]:

**Battery zone:** Due to its unique requirement for a low and tightly specified temperature range [0°C;40°C], the battery module is isolated from the rest of the platform. This is achieved by employing an internal MLI covering the entire panel and the battery itself, along with insulating washers that isolate the -Z panel from the rest of the frame. Additionally, a robust conductive coupling between the battery and its radiator, facilitated by an aluminum doubler, enhances the rejection of dissipated heat through the SSM radiator.

**Propulsion zone:** Due to the stringent temperature requirements of the hydrazine liquid and the low thermal conductivity of titanium tubing, the thermal control of the propulsion zone emerges as the most critical aspect. All components filled with hydrazine are connected to the -Xs panel, which is maintained within the [15°C;38°C] [106] temperature range. This significantly simplifies the heating system of the propulsion zone. An internal MLI covers the tank, the upper side of the -Xs panel, and all hydrazine-filled components located on the upper side of the propulsion panel, thus limiting radiative coupling with the rest of the platform.

**Platform main zone:** Disregarding the specific passive thermal control of the bottom frame, the heat rejection for the platform main zone is achieved thanks to 3 SSM coatings bonded on the honeycomb structure of the lateral panels. Except for these radiative surfaces, the whole platform is covered with external MLI. The inner parts of the lateral panels and all the internal units are black painted to homogenize as much as possible the temperature in the platform main zone. This is also achieved by conductive coupling between the different lateral panels through the frame, conductive coupling between the internal units and their mounting panel through thermal fillers for most of them, and an aluminum doubler between the DHU and its panel.

**Star-tracker module:** To easily maintain the alignment of the Star-trackers with the payload despite thermo-elastic loads, they're positioned in an autonomous module situated on the external side of the Anti-Earth panel of the Payload module where temperatures are kept between 5°C and 30°C. [106] The 2 Star-trackers are connected to the same plate to benefit from cold redundancy where the "off" unit cools down the "on" unit and vice versa, the heat dissipated by the "on" unit is directed towards the radiator through an aluminum doubler. The warming up of the 2 units is facilitated by a single heating line located on the common thermal plate.

**Payload module:** The payload module is positioned on the top surface of the platform. Its connection to the platform is facilitated by titanium tubes situated at the four corners of the frame. This method of attachment accomplishes two objectives: firstly, it provides the necessary conductive uncoupling, thereby enabling separate thermal control sizing. Secondly, the payload can utilize 11 regulated heating lines supplied by the platform for its thermal requirements.

## 3 External and Internal heat fluxes along the phases

### 3.1 External flux

Jason-2 maintains this orbit throughout all of its operational lifetime, with only minor adjustments ( $\pm 10$  km) that do not affect the external heat flux trend. It can therefore be assumed that the thermal variations remain constant throughout the mission.

Since the inclination of the Jason-2 orbit is of 66°, large changes in lighting conditions and therefore external heat fluxes are experienced by the satellite. The angle between the sun and the orbital plane can vary from 0° to 90°; this represents a serious constraint for the thermal control performances: the larger the variation, the greater the thermal heating power required to keep all components in their correct temperature range. The hot case occurs at an angle of 60° with respect to the sun (first orbits without eclipse); whilst the cold case occurs at around 0° (maximal eclipse). [106]

To cope with this conditions, a Yaw steering manoeuvre is applied that on top of allowing the solar panels to be perpendicular to the sun, takes advantage of the shade to reduce the heat fluxes thanks to the non-illumination of the [+/-Ys] and [-Zs] faces.

### 3.2 Internal fluxes

During the launch phase, internal fluxes are not present due to the fact that the electronics are turned off. This changes in the Early orbit phase, once the solar arrays are deployed and the satellite becomes operative. The flux presence is correlated to the data uplink and downlink, along with the Earth observation measurements which are conducted throughout the satellite lifespan to ensure continuity in retrieved observation data and transmission. Internal fluxes remain present throughout the operational life of Jason-2 until the decommissioning phase, and they vary depending on the various modes.

In nominal operating mode all the sensors and payloads are activated and operational, so their heat fluxes are present together with the flux coming from the batteries units. When transitioning to safe-hold mode, the spacecraft must adopt an energy-saving configuration. While the star trackers remain active, the main platform sensors switch to a less demanding configuration and the batteries discharge only a portion of their nominal power. Consequently, a noticeable decrease in internal flux is expected.

## 4 Requested temperature intervals

Hereby the temperature ranges for the principal components of the Jason-2 spacecraft are presented in Table 32. Temperature limits are eventually related to the adoption of thermal control strategies.

Equipment	Performed range		Operating range	
	$T_{min}$ [°C]	$T_{max}$ [°C]	$T_{min}$ [°C]	$T_{max}$ [°C]
Average equipments[53]	N/A	N/A	-20	50
Electronics[106]	0	35	-10	50
Battery[88]	22	30	0	<b>40</b>
GPS[2]	-5	28	-10	50
TTC[2]	2	40	-10	50
DHU[2]	8	42	-20	50
STR[106]	5	30	0	<b>40</b>
$N_2H_4$ Filled components[2]	15	38	<b>10</b>	50
Solar array[100]	N/A	N/A	-100	95

Table 32: Thermal Budget

The most stringent cold limit is imposed by the hydrazine tanks, requiring the highest power from heaters to prevent propellant freezing, whereas the most stringent hot limit applies to the battery and star trackers.

## 5 TCS Sizing

The thermal control system (TCS) sizing was conducted using a preliminary, mono-node, and steady-state analysis. Initially, the environment was modeled to identify the most extreme hot and cold scenarios throughout the entire mission duration. Subsequently, leveraging the energy balance, the surface area of the radiators and the power of the heaters were determined to ensure the maintenance of the desired temperature range.

### 5.1 Environment modeling

The environment was studied modeling four principal sources of thermal energy in order to determine the most extreme hot and cold scenarios.

**Sun radiation:** because of its low altitude, the distance between the satellite and the Sun was presumed to be of 1 AU. However, this contribution was not considered in the cold case scenario, as during an eclipse, there is an absence of solar radiation.

**Albedo:** being a consequence of the Sun radiation, it has to be considered only in the hot case scenario. In a more detailed analysis, this contribution should be recognized as non-constant throughout the orbit. In fact, Jason-2 orbit spans a latitude range of  $\pm 66^\circ$ [3] causing the Albedo contribution to vary from a maximum, at the highest latitudes, to a minimum, at the equatorial plane.[70] However, to ease the computational burden of the simulation this variation was disregarded and the computation of the Albedo flux will be described in more details in subsection 5.2.

**Infrared:** similarly to the Albedo contribution, it has a dependency on the spacecraft latitude; it is maximum at the equator and minimum at the highest latitude. Also in this case, a constant value was picked, neglecting this variability as it is generally complex to compute. Furthermore, this heat source is present in both the cold and hot case as it emitted from Earth, approximating its radiation as a grey body.

**Internal:** the internal dissipated power is closely linked to the modes and phases of the Jason-2 mission as explain in subsection 3.2.

Another significant consideration is the degradation effect inherent in a low Earth orbit (LEO) and, more generally, solar exposure. Specifically, the mission was launched during a period of minimal solar activity, which intensified over the satellite's lifespan. It means that, as Jason-2 prolonged its time in orbit, its optical properties experienced substantial deterioration due to the cumulative impact of prolonged exposure to the harsh environment of a LEO orbit and the escalating solar activity over time. [73]

The operational temperature range was determined to be from -20°C to 50°C, based on average equipment requirements as outlined in Table 32. The reason is that most of the electronics, including the different sensors, can operate in the aforementioned range. Furthermore, a margin of  $\pm 15K$  was applied to this values, due to the preliminary of the analysis in accordance with MAR-TCS-010.[20] Thus, the new operating margin was -5 °C to 35 °C. In a further analysis, a non homogeneous temperature should be considered, along with the specific needs of the most restricting components which are the hydrazine tank, the battery and the star trackers.

### 5.1.1 Material selection and coating

The analysis proceeded under the assumption that the whole satellite is covered with MLI whose outer layer is a gold-colored kapton material.[68] This assumption is justifiable given that Jason-2's surface is mainly covered by this thermal blanket, except for the radiator surfaces, which are relatively small in comparison to the overall surface area. The optical properties of this MLI layer allow the spacecraft to keep a stable temperature. [100] For simplicity, the following analysis neglects any degradation due to the environment, which for a satellite in LEO for a nominal duration of 5 years would lead to an increase of 0.09 in absorvivity.[50]

Jason-2 mission uses SSMs for its radiators as they allow to effectively combine the high emissivity of the upper surface with the high reflectivity of the lower surface resulting in a radiative surface that optimizes emission while minimizing the absorption of external heat.

Material	$\alpha [-]$	$\varepsilon [-]$
Kapton[31]	0.23	0.03
SSM[100]	0.16	0.76
Solar Array-cell face[100]	0.85	0.82
Solar Array-back face[100]	0.92	0.7

Table 33: Materials optical properties

As the solar arrays were analyzed separately, the characteristics of both faces were considered and the values were retrieved from literature.

## 5.2 Hot case sizing

The worst hot case scenario occurs during the Extended Routine Operations Phase when all payloads and sensors are active, resulting in a maximum internal energy source. Additionally, all external heat sources are present during this phase. The hot case heat fluxes are presented in Table 34.

$Q_{int,max}$ [W]	$Q_{Sun}$ [W]	$Q_{albedo}$ [W]	$Q_{IR}$ [W]	$T_{sc,hot}$ [°C]
457	312	451	25	223

Table 34: Hot case heat fluxes and satellite temperature

The heat fluxes were calculated considering the different surfaces impinged by the heat fluxes under the following assumptions:

- $Q_{int,max}$ : the internal generated power was evaluated summing the dissipated power by the platform in nominal conditions (310W)[2] and the power input of the payloads (147W)[27]. Due to the lack of available information regarding the dissipated power of the payloads, it was determined to adopt the worst-case scenario where all power input is assumed to be converted into dissipated power. Overall, the total dissipated internal power amounts to 457 W. No further margin were applied, as the latter assumption will already lead to a reasonable value for the sizing.

- $Q_{Sun}$ : the solar flux was computed considering  $q_0$  equal to  $1358 \frac{W}{m^2}$  and the absorbitivity coefficient  $\alpha$  was set in subsection 5.1. An area of  $1m^2$  was considered as the one parallel to the solar array, under the assumption of Nadir-pointing mission as explained in subsection 5.1.

- $Q_{albedo}$ : since the Jason-2 mission performs Nadir-pointing, the area considered was the Earth pointing surface equal to  $3.7m^2$ . The Albedo coefficient of Earth was picked equal to 0.39, from the range 0.31-0.39 for conservative sizing and the Albedo factor equal to 1.[50]

- $Q_{IR}$ : the infrared power was computed defining  $\epsilon_{Earth} = 0.95$ [46] and the planet's temperature  $T_{pl} = 255K$  which is its black body temperature. As in the Albedo case, the area considered is  $3.7m^2$ , while the emissivity of the spacecraft is chosen as stated in subsubsection 5.1.1.

Once the powers were computed, the temperature of the spacecraft in the hot case was recovered by solving the heat transfer balance between the internal and external energy sources and the emitted power. In particular, the emitted power towards the DS was evaluated by assuming an area equal to the remaining one with respect to the surfaces that were already impinged by the external heat sources, leading to  $12.1m^2$  and with the previously defined optical properties. Lastly, the DS temperature was set to  $T_{dp} = 3K$ .

The output of the simulation lead to an unacceptable  $T_{sc,hot}$  which is outside the defined upper thermal boundary. Thus, a passive control strategy was evaluated. The high value obtained can be attributed to the inherent approximations of the model and the numerous assumptions regarding surfaces, optical properties, and power.

### 5.2.1 Radiator sizing

Since the outcoming temperature of the hot case turned out to be major than  $35^\circ C$ , it was necessary to size radiators in order to dissipate the heat power in excess and reach the wanted operating temperature.

Fixing a desired  $T_{sc,max}$  to  $35^\circ C$  and assuming the emissivity of the radiators from Table 33, through the balance of heat powers it was possible to recover the minimum radiator area to guarantee this temperature. From this preliminary analysis a required area of  $A_{rad} = 2.81m^2$  was obtained. This is a reasonable value as it is the 17% of the total surface of the Jason-2 spacecraft, further supporting the assumption that the majority of the surface is wrapped in the MLI. This value is higher than the actual total area of the radiators in the Jason-2 mission as it is reported that it is  $1.9m^2$ .[40] The discrepancy can be related to the assumptions on the value of the internal power, the surfaces that are impinged by radiation and by the applied margins.

## 5.3 Cold case

The worst cold case scenario is outlined during the Launch and Early Orbit Phase where the main payloads are switched off and a SHM is triggered. In terms of internal power this is the worst case as there is a minimum of only  $180W$  internally dissipated by the platform.[106] Moreover, during eclipse, in this condition, the only external heat source is the infrared radiation incoming from Earth. The area considered for the infrared radiation is the area of the Nadir-pointing surface ( $3.7m^2$ ), while the surfaces that dissipate towards the deep space are the remaining ones ( $13.1m^2$  in total) from which the area of the radiators was subtracted.

$Q_{int,min}$ [W]	$Q_{IR}$ [W]	$T_{sc,cold}$ [ $^\circ C$ ]
180	25	-77

Table 35: Cold case heat fluxes and satellite temperature

As can be observed in Table 35,  $T_{sc,cold}$  is not acceptable, being well below the lower bound of the set thermal boundary. It was then necessary sizing an active control mechanism which in this case involved sizing heaters.

### 5.3.1 Heater sizing

As the resulting temperature from the cold case was lower than  $-5^\circ C$ , heaters were sized in order to reach the wanted minimum temperature. The power required was computed with a thermal balance which fixed the desired s/c temperature at  $-5^\circ C$ . Thus a power of  $Q_{heaters} = 518 W$  is required. This value is much higher than the one found in the literature ( $180 W$  [19]). This can be related to the underestimation of the internal dissipated power of the platform during the SHM, the hypothesis on the dissipating areas and, most importantly, on the most restricting temperature to be reached. Furthermore, the assumptions of mono-nodal and steady state analysis lead to a very preliminary computation that can diverge significantly from the real values.

Taking the total power required from the sizing and considering that the average power for the heater is  $8.6 W$  - this value comes from subsection 1.2 where we have a total power of  $180 W$  and 21 heaters. Thus, the number of heaters needed is 61 but this value needs to be doubled to account for cold redundancy. The total number for heaters is then 122. This value significantly exceeds the real value of 42 heating lines reported in literature. 1.2 The number of heaters computed with the sizing is three times higher than the real value since the needed heating power is three times the one from literature.

## 5.4 Specifically controlled units

A further analysis was conducted on the solar arrays to ascertain whether they remain within the optimal operating temperature range reported in Table 32 during nominal conditions, specifically throughout the Initial Routine Operations Phase and the Extended Routine Phase. This analysis aimed to establish a thermal control strategy in the event of overheating or freezing. The study was conducted separately from the satellite since the panels do not directly dissipate heat towards the surfaces of Jason-2 and can be considered thermally isolated from the satellite.

The solar array was modeled as a flat plate, and subsequently, the temperatures were calculated for both the hot side (facing the Sun) and the cold side (facing deep space). The heat powers were computed using the emissivity and absorbivity values defined in Table 33. The heat fluxes impacting the hot side consist of solar and Albedo fluxes, while the cold side receives radiation from Earth, thus necessitating the application of their respective optical properties in the calculation of flat plate temperatures.[50] Moreover, the panel efficiency was assumed to be 0.3, a typical value at the BOL.[50]

$A[m^2]$	$Q_{\text{Sun}} [\text{W}]$	$Q_{\text{Albedo}} [\text{W}]$	$Q_{\text{IR}} [\text{W}]$	$T_{\text{pan,hot}} [{}^\circ\text{C}]$	$T_{\text{pan,cold}} [{}^\circ\text{C}]$
4.9	5656	2206	781	85	-66

Table 36: Mono-nodal analysis on solar arrays

The results show that the temperatures for both the hot side and cold side fall within the specified operating range; the MAR-TCS-010 [110] was not applied since the temperature ranges are those taken from the Jason-2 mission manual.[100]. The results are deemed reasonable as the flat plate approximation, even under a mono-nodal analysis, effectively captured the behaviour of the solar arrays.

Additional critical components that influence the thermal behaviour of Jason-2 include the hydrazine tank, the star trackers, and the batteries. Given their narrow operational ranges, a multi-nodal analysis is necessary for a detailed characterization.

## 5.5 Adopted control strategy

From the evaluation of the temperatures, a passive control was initially implemented due to the cost and complexity associated with active control, reserving it as a final option. However, in the worst cold case it was necessary to implement such control. Implementing a more specialized coating or painting to increase temperature was not feasible, as the only parameter affecting the eclipse was the emissivity in the infrared band.

Differently, in the worst hot case, it was possible to manage the excess heat by integrating SSM. Their efficacy resides in their high emissivity that allowed to dedicate a small surface area to reach such dissipating effect.

## 5.6 Position and pointing

The radiators are directly positioned as panels on the satellite's surface facing the deep space and orthogonal to the solar arrays, so that a correct disposal of the excessive heat is granted. The payloads' DHU and the satellite's batteries have to be placed respectively on the Earth panel and the Anti-Earth panel, directly on the radiators.[2] While, for those type of components that cannot be arranged in such a way, braids and straps have to be included in the subsystem to create a thermal bridge that connects those elements with the radiators. The heating lines are positioned inside the platform to heat up the most critical components, which are principally the batteries, star trackers and the hydrazine tank. Moreover, as a parallel solution with heaters, those components are to be wrapped in MLI to decouple them from the satellite environment. Those considerations could be further improved with a multi-nodal analysis which accounts for the different requirements of the Jason-2 components.

## 5.7 Subsystem budget

The mass and power budget are reported in Table 43 along with the relative error between the real and the computed values.

	Real	Computed	Error
Mass [kg]	12.2 [35]	18.4	51%
Power [W]	180	518	188 %

Table 37: TCS mass and power budget

The total mass budget is computed by taking 3.5% of the overall dry mass of the satellite, which amounts to 525 kg.[10] This derived value aligns well with the real data, given that a percentage range between 2 and 5 is considered acceptable.[80]

Regarding the power budget, it primarily consists of the power needed for the heaters, since the cooling system operates passively in the hot case. However, the computed value from the sizing appears to be unreasonable, likely due to the simplicity of the model used for sizing. The substantial relative error further underscores the inadequacy of the model in providing an accurate estimate. The TCS data is managed by the On-Board Data Handling Unit of the PROTEUS platform, which triggers the activation of heating lines based on input from the thermistors.

# **Homework 6**

## **Electric Power Subsystem**

# 1 EPS Architecture

The Electric Power System has the role of generating, storing and distributing the spacecraft's power throughout the whole mission lifetime. Jason-2 makes use of the electrical power architecture provided by the multimission PROTEUS platform, with specific adaptations to match the power required by the payload. The EPS interfaces with both the TCS, given the thermal fluxes, and the AOCS for solar panels orientation.

## 1.1 Primary Power Source: Solar Arrays

For near-Sun (Earth orbit or closer) and long missions (years) like Jason-2, solar photovoltaic is the most reasonable choice for a power source. This is because, at these distances, the power density of sunlight is sufficient for the production of electricity for a LEO satellite. More specifically, at 1AU the irradiance of the Sun on the outer Earth atmosphere is  $1358 \text{ W m}^{-2}$ .[107] [23] The primary power source for the Jason-2 mission is, therefore, a set of two solar arrays that are extended in orbit on opposite sides of the satellite's main platform. To allow pitching of the solar arrays to point the sun without changing the attitude of the payload, two single-axis stepping motordrives are employed.[100] Each array consists of four  $1.5 \times 0.8 \text{ m}$  panels covered with silicon cells, making up a total area of  $9.5 \text{ m}^2$ .[68, 100] Silicon cells make up the arrays with the addition of coverglass and adhesives. The selection of this technology over multi-junction cells was motivated by a mass, cost, and simplicity advantage.[25] The solar array wingspan when fully deployed measures 9.7m from tip to tip. Overall, this power source can generate between 500W and 900W.[68]

This is the only primary power source in the satellite, something that is possible due to the shortness of the eclipse phases, and the use of a secondary rechargeable battery, as shown in subsection 1.2.

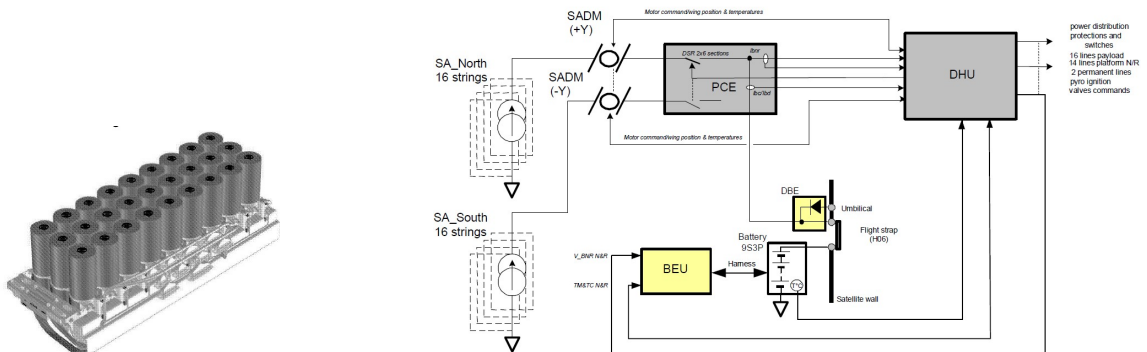
## 1.2 Energy Storage: Secondary Battery

During eclipses, power is provided by a secondary battery.[68] Unlike the preceding Jason-1 mission that used a 40 Ah Ni-Cd battery, Jason-2 makes use of a 78 Ah Li-Ion developed by SAFT (VES100).[100] This change was made to satisfy larger payload needs in terms of power, and increase the storage capacity, especially during the Safe Hold Mode.[81] The battery is composed of 9 cell packages connected in series, and each cell package is made of 3 cells connected in parallel (9s 3p technology). This adds up to a total of 27 cells, with a weight of 0.81kg each. Each cell package has a by-pass, which is a safety device used in case of cell overvoltage or undervoltage. Additionally, 18 shunts (9 nominal and 9 redundant) are present to ensure the cell package balancing function; these are resistive devices ( $\approx 20 \Omega$ ) that compensate for the variation of state of charge among all the cell packages of the battery.[89]

The VES100 battery can operate in any orientation and is compliant with the ESA Procedure and Specification Standards (PSS). The long cycle life is 70,000 LEO cycles at 20%, which corresponds to approximately 14 years.[89] A representation of the battery and the single cell can be seen in Figure 17a.

## 1.3 Power Control and Distribution

Distribution and regulation are important to deal with the different load requirements, variability of the mission profile, power source degradation, and battery charge/discharge control. For Jason-2, power is distributed through a single non-regulated primary electrical bus (23/36V with an average 28V voltage), with digital control performed by the data handling unit (DHU) through proportional commands.[81] According to these control commands, the Power Conditioning Equipment (PCE) controls the battery state of charge by delivering the required charge current. Additionally, there is a Battery Electronic Unit (BEU) that delivers the required cell voltage acquisition used as an indication of the individual cell state of charge.[4] An overview of the architecture of the power control is shown in Figure 17b.



(a) SAFT VES 100 78 A.h Lithium Ion Battery. [81]

(b) Power control architecture. [4]

Figure 17: EPS architecture.

## 2 EPS architecture according to Phases/Modes

The EPS architecture presented above can be justified by looking at the electrical power requested by the Jason-2 subsystems along the mission. Different phases don't show varying power requirements, except for the launch and early orbit phase. On the contrary, different modes in Jason-2 can be analyzed to observe changes in the power requirements.

### 2.1 Power requirements per modes

During the mission, Jason-2 undergoes four different main modes:

- **Normal Operation Mode:** in addition to the vital satellite management functions, all the specific payload requests have to be taken into account leading to a maximum consumed payload power of 147 W. Commanding and status are provided via 1553B bus.[100] Regarding the specific subsystems, the only ones to be inactive are the propulsive one and, during sunlit, the thermal control. Complexly, a total of 444.4 W is provided.
- **Orbit Control Mode:** in this mode the thrusters are used and consequently it leads to a power request by the propulsion system. The performances and services are the same as in Nominal mode, but payload functioning can be restricted during large manoeuvres. The periodicity and the choice of these modes depend on specific mission analysis and control. [100] This mode is the most demanding, with a total of 540.5 W requested.
- **Safe Hold Mode:** in this mode, the platform provides a minimum amount of power to satisfy only the vital functions of the satellite. It includes ground to s/c communication, thermal control, battery management, failure management and coarse sun pointing. The maximum payload power in this mode is 30 W.[100] From these considerations, the mean value of the demanded power in SHM can be computed as 232.4 W.
- **Star Acquisition Mode:** In this mode, the payload operations are restricted to the ones strictly necessary to verify the instruments behaviour. The payload nominally is turned off, but in case of special needs 2 of the 16 power lines can be maintained on, which can drain a maximum of 30 W.[100] The resulting requested power is estimated equal to 328.4 W.

The power budgets divided by the subsystems and by modes are tabulated hereafter. The values used are taken from the power budgets computed for the different subsystems in the previous assignments and by the PROTEUS platform manual.

Mean Power demand [W]	NOM	OCM	SHM	STAM
PS	0	96.1	0	0
TTMTC	97.5	97.5	100	97.5
ADCS	199.9	199.9	102.4	200.9
TCS	0	0	0	0
PL	147	147	30 [100]	30 [100]
Total	444.4	540.5	232.4	328.4

Table 38: Power budget per mode.

In Table 38 a sunlit condition is assumed and therefore there is no TCS requested power, as in this condition the satellite performs passive control. The value of the required power demand during eclipse is 250 W from literature. Most of this power is provided to the TCS which consumes up to 180 for active thermal control.[95]

This results shown in Table 38 justify the selection of solar arrays as primary power source since all modes have a power demand that is compliant with the range of generated power of 500 W - 900 W.

## 3 Operational profiles and available sources

Power sources can be divided into primary and secondary ones: the only primary power sources in the satellite are the solar arrays, which is feasible due to the shortness of the eclipse phases, and the use of a secondary rechargeable Li-Ion battery, as shown in subsection 1.2. The aim of the secondary power source is to supply energy during primary source unavailability or to support potential peak power demands. Since the satellite orbit is around the Earth and does not change significantly during Jason-2 operational period, it can be assumed that the energy coming from the Sun is always available except during eclipses.[68] Figure 18 shows the percent of Jason 1 and 2 orbits in eclipse, knowing that the two satellites follow the same path. Depending on solar aspect angle, eclipses duration vary from 0 to 35 minutes which approximately represents a percentage ranging

from 0 to 30%. [81, 85] The change in lighting conditions is caused by the fact that the orbit of Jason-2, with an inclination of 66 °, is subject to a solar drift of -3 °/day. [81]

**Battery voltage:** Figure 19 shows the results of a test carried out on nine VES100S cells. Its objective was to characterize the long term behaviour of VES100 under LEO cycling conditions at different End of Charge voltages (3.85V, 3.95V, 4.05V). In the figure is shown as, after four years of real time cycling (greater than 20000 cycles), the cell voltages are nominal. [111] The positive outcome of this test justifies the use of these batteries for Jason-2, considering an expected mission duration of 5 years.

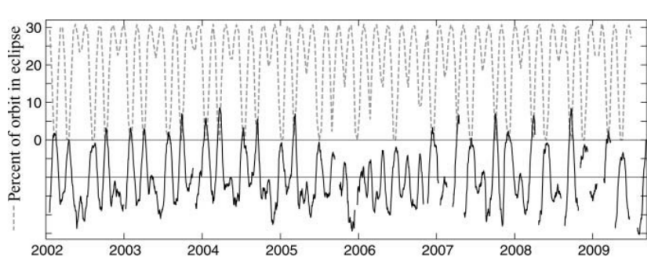


Figure 18: Percent of Jason-1 orbit in eclipse. [85]

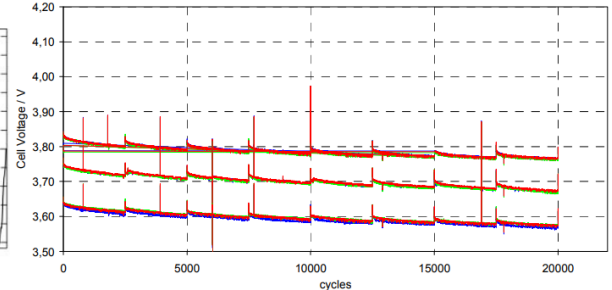


Figure 19: Long term behaviour of VES100 cells. [111]

**Solar arrays orientation:** in the free yaw case, the attitude of the satellite follows a yaw steering to orient the solar arrays towards the Sun, following a near sinusoidal movement along the orbital period. [100] This change in the SA orientation, combined with the motordrives mentioned in subsection 1.1, aims to avoid power losses and to optimize the use of the available Solar power.

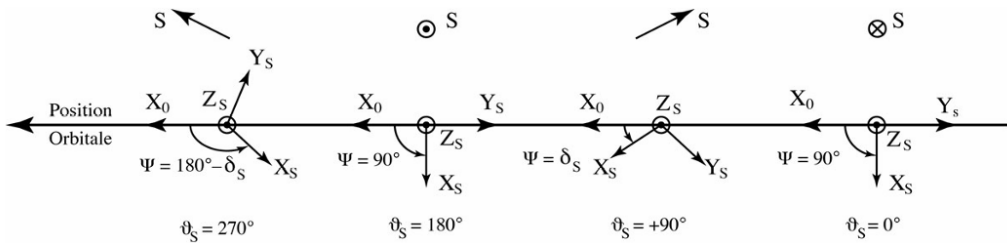


Figure 20: Solar arrays yaw steering. [100]

### 3.1 Payload power profile in early orbit phase

In Figure 21 a typical evolution of the available power drained from the platform PROTEUS to the payloads after launch phase is represented.

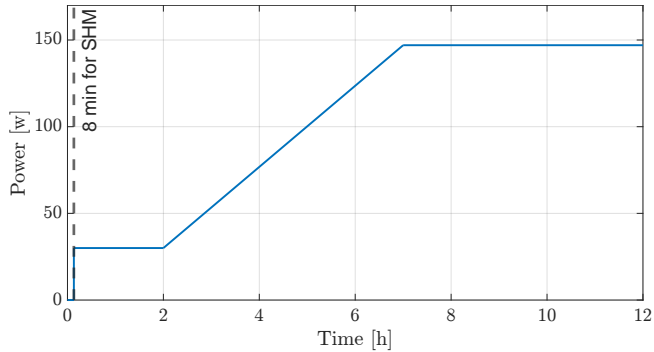


Figure 21: Timing of typical 1553 exchanges between platform and payload. [100]

In the first 8 minutes after separation from the launch vehicle, the satellite enters a SHM in which the payloads are still turned off and the requested power is 0 W. At the end of this mode, the satellite starts to drain power to the payloads. [100] The available power grows over the next hours until it reaches a nominal average condition of 147 W available.

## 4 EPS Sizing

The sizing of the EPS subsystem began with analyzing the power budget for each subsystem in every mode of the mission. After identifying the most demanding modes in terms of power consumption, the primary energy source was sized accordingly. Additionally, a secondary source was sized to accommodate potential peaks in power demand, failures, or unavailability of the primary source.

### 4.1 Power Budget per mode

Starting from the power budget for each mode computed in Table 38, a margin of 20% was applied on the total power demand for the sizing according to the MAR-PWR-040.[20] The results are shown in Table 39

Mean Power demand [W]	NOM	OCM	SHM	STAM
Total	444.4	540.5	232.4	328.4
+20% Margin	88.9	108.1	46.5	65.7
Total margined	533.3	<b>648.6</b>	278.9	394.1

Table 39: Power budget per mode with margins.

From this table, it is possible to identify the least and most demanding modes throughout the mission. The total power request for the OCM, being the most demanding, was used as the maximum power required in daylight. This value matches perfectly with the real value for sunlit conditions found in the literature  $P_d = 540\text{W}$ . [95] Since no information was available for the power demand during eclipses, the sizing was performed using the literature value of  $P_e = 250\text{W}$  [95], which is associated with the nominal operating condition during an eclipse. Both values were margined according to MAR-PWR-040.[55]

### 4.2 Primary source selection and sizing

The primary energy source was chosen to be photovoltaic due to the close proximity to the Sun (1 AU), which results in a high specific power for the solar arrays. This choice is further supported by the mission's nominal duration; according to the literature, for a duration of 5 years, a photovoltaic solution is preferred. [80]

In order to size a Solar Array system several information are needed:

$T_d[\text{min}]$	$T_e[\text{min}]$	$X_d[-]$	$X_e[-]$	$P_d[\text{W}]$	$P_e[\text{W}]$	$I_D[-]$	$d_{py}[-]$	$\epsilon_{BOL}[-]$
77.6	34.8	0.85 [50]	0.65 [50]	648.6	300	0.88 [51]	0.0275 [51]	0.094

Table 40: SA sizing parameters.

$V_{cell} [\text{V}]$	$V_{sys} [\text{V}]$	$A_{cell} [\text{cm}^2]$
2.6	28	23.61

Table 41: SA refined sizing parameters.

The time spent in daylight and in eclipse were computed using a simplified approximation that produced reasonable values for a LEO orbit, closely matching those of the actual mission.[95]. The coefficients  $X_d$  and  $X_e$  were assumed based on the power control strategy used, which was Direct Energy Transfer (DET), as further detailed in subsection 4.4. The values of the inherent degradation factor ( $I_D$ ) and yearly degradation ( $d_{py}$ ) are those for Si cells, which are used in Jason-2 panels. The efficiency at beginning of life ( $\epsilon_{BOL}$ ) was retrieved from Figure 22 considering the value corresponding to the highest operating temperature of the solar arrays  $T=95\text{ }^\circ\text{C}$ .[100] Knowing the structure and thickness of the cell layers, an average density for silicon cells was computed ( $\rho_{SA} = 0.3351\text{m}^2/\text{kg}$ ).[43]

The first step involved computing the power required by the solar arrays using the power data from Table 42. Next, the specific power at BOL was calculated assuming a solar flux of  $1358\frac{\text{W}}{\text{m}^2}$  at 1 AU and an average inclination angle of  $23.44^\circ$  between the normal to the panels and the direction of the Sun.[14]

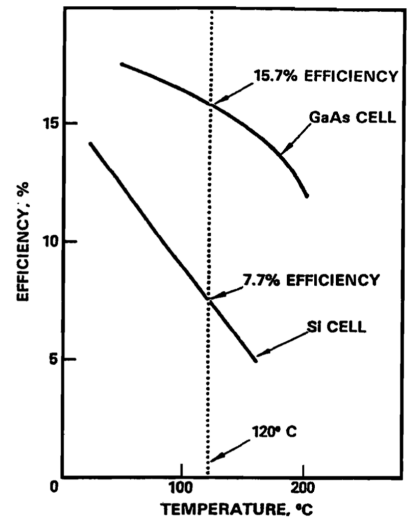


Figure 22: Si cells BOL efficiency.[106]

Moreover, to assess the degradation of the panels, the solar array degradation factor ( $L_{life}$ ) was calculated considering the duration of the mission to be 5 years. The specific power at EOL was determined and the solar arrays area was computed. In order to grant the necessary power to the platform even in the event of a string failure, one string was added to this last result.

The area of this string was computed as the product of the total arrays' length (12 m) times the height of a cell (4.86 cm). [93] Furthermore, a refined sizing was conducted to obtain more precise values for the solar array mass and area.

	$m_{SA}[\text{kg}]$	$A_{SA}[\text{m}^2]$	$P_{SA}[\text{W}]$
Computed value	34.02	11.4	970
Real value	28.35	9.5	900
Relative error	16.7%	20%	7.8%

Table 42: SA sizing results.

Since we are sizing for the most power demanding conditions, the value of 900 W is taken as the upper bound of the range from subsection 2.1.

The results in Table 42 are obtained considering an average inclination angle between the Sun and the solar arrays as the most conservative option. In reality, since the solar arrays are provided with a pitching mechanism, the cosine of the angle should tend to unity. Performing the sizing with a 0° angle, the mass and area computed show a smaller relative error with respect to the real values.

### 4.3 Secondary source selection and sizing

To supply energy during primary source unavailability and to support peak power demands, a secondary power source was selected. Despite the satellite operating in standard conditions, a Li-ion battery was chosen. These batteries exhibit excellent performance and do not require reconditioning. They also have one of the highest energy densities and specify energies among secondary batteries [51], meaning they can store a significant amount of energy relative to their weight and volume. The high cell voltage allows for fewer batteries to be stored onboard. Li-ion batteries have been widely used in various space missions, proving their reliability and effectiveness.

To size the battery, the following information was required:

$T_R[\text{min}]$	$P_R[\text{W}]$	$E_m[\text{Wh/kg}]$	$E_v[\text{Wh/dm}^3]$	$\eta[-]$
34.8	648	118 [89]	230 [89]	0.65

Table 43: Battery sizing parameters.

$T_r$  is the time window during which the battery must provide power, assumed to be equal to the eclipse duration. Since the battery needs to be able to supply energy in the event of primary source unavailability, the computation of the required power,  $P_R$ , was conducted considering the most critical demand obtained in Table 38. The line efficiency was assumed to be equal to that of the solar array, with the lower eclipse value used for conservative reasons.

First, the required capacity to meet the power demand was computed, considering 1 battery with a DoD of 40% which is at the lower end of the typical value range.[51]. Next, a refined battery sizing was performed to ensure the spacecraft's power needs could be met even in the event of a cell failure. The nominal system voltage,  $V_{sys}$ , to be provided is 28 V [100]. To account for a cell failure,  $V_{sys}$  was taken as 32.4 V, computed as  $N_{series} \cdot V_{cell}$  where  $N_{series} = 9$  as showed in subsection 1.2 and  $V_{cell} = 3.6$  V [89]. A package efficiency of 80% was considered.[51] The results are shown in Table 44.

	$mass_{cell}[\text{kg}]$	$Vol_{cell}[\text{dm}^3]$	$C_{sys}[\text{Wh}]$	$N_{series}[-]$	$N_{parallel}[-]$
Computed value	0.45	0.23	2099.5	9	3
Real value	0.81 [89]	0.41 [89]	1814.4	9	3
Relative Error	44%	44%	16%	-	-

Table 44: Battery sizing results.

The cell mass was computed because no information was available about the total battery mass, which would have included wiring, casing, and insulation, leading to a higher error margin. The same approach was applied to the volume computation where the real cell volume was computed from the cells dimension  $d_{cell} = 5.3\text{cm}$  and  $h_{cell} = 18.5\text{cm}$ .[89] A higher system capacity than the desired one was obtained; to refine the design, a cell with a lower capacity but the same voltage could be selected. The topology matches the actual one used, considering the necessary redundancy.

#### 4.4 Primary source regulation adopted strategy

A Direct Energy Transfer (DET) design features a shunt regulator in parallel with the solar array, which shunts excess power back through the array for dissipation into space. [51] In this configuration, both the solar array and the battery are connected directly to the bus. This arrangement means that the solar array's power output is dependent on the battery's state of charge. To prevent overcharging, any excess power is dissipated through the shunt regulator. This architecture's direct connections between components ensure that the system's overall efficiency is nearly unity, regardless of light conditions. [48]

The DET system is particularly advantageous for space missions with few eclipses and stable operating conditions. In such scenarios, the minimal losses associated with DET converters can offset the potential benefits of Peak Power Tracking (PPT) systems. PPT systems, while efficient in variable conditions, introduce additional complexity and potential points of failure. Consequently, DET converters are often preferred for missions where power stability and simplicity are paramount. This preference is due to the inherent efficiency and reliability of the DET design, which maintains high performance with fewer components and simpler control mechanisms. [48]

#### 4.5 Bus regulation adopted strategy

The power is distributed through a single non-regulated primary electrical bus, where the voltage is not actively regulated. The main energy source directly feeds the platform.

This choice was made for the simplicity of the architecture and hardware. An unregulated power bus is suitable for this mission because the solar arrays provide a constant power input under sunlit conditions, thanks to the solar array pitching mechanism and the consistent distance to the Sun throughout the mission. [100]

#### 4.6 Positioning of components and pointing requirements

When stowed, the panels are compactly folded against the satellite. Upon deployment, they are positioned to grant sunlight exposure for optimal power generation. The solar arrays consist of two deployed 4-panel wings connected to the  $\pm Y$  sides of the S/C bus via structural support. These panels can be rotated around the pitch axis using electrical motors, ensuring they align with the Sun at different offset angles. This alignment keeps the surface perpendicular to the sun rays at different inclination angles, guaranteeing proper temperature and power regulation. [100]

The batteries are located on the -Z face (Anti-Earth panel) and are thermally uncoupled from the rest of the platform. They are efficiently integrated with thermal control systems to dissipate heat generated during charging and discharging cycles. The batteries are positioned close to the DHU to minimize power losses and ensure efficient power management. This proximity helps maintaining high efficiency and reduces the complexity of power cables. [2]

#### 4.7 Subsystem budget

The mass, power, and volume budget for the EPS subsystem is presented below and compared to the actual values. The computed total mass is the sum of the battery mass, the solar arrays, and the cabling and harness mass. The cabling and harness mass is considered to be 20% of the total EPS mass, which is the average value within the possible range of 15%-25%. [51] The power computed is taken from literature as a typical value for conditioning: 20.2W.[51] A 20% margin was added to this value, as it is based on data retrieved from literature.[20] The computed volume budget comes from the solar arrays area computed from the sizing while considering a thickness of the solar cell to be 200  $\mu m$ . [93] The volume of the battery computed in the sizing is added to it. The same procedure was adopted for the computation of the real volume using the solar array area and battery volume retrieved from literature. The volume of the harness and the cables was not considered.

	Real	Computed	Error
Mass [kg]	84	57.8	31.2%
Power [W]	27	24.24	10.2%
Volume [ $dm^3$ ]	12.92	8.56	34%

Table 45: EPS mass, power, and volume budget.

The computed total mass shows a discrepancy with the real mass value which was considered to be the 16% of the total mass.[55] This difference may be due to the fact that the battery mass is computed simply as the sum of the cells weights without considering the case or any internal apparel. Similar considerations can be applied to the volume difference. The computed power budget is close to the real value which is considered to be 5% [51] of the total power request. At last, the data budget is comprised of the measurements of the current, voltage, rates of charge-discharge of the battery through the appropriate sensors. Furthermore, the data coming from the different electrical interfaces, the switches and the relays is also accounted.

# **Homework 7**

## **Configuration & On-Board Data Handling**

# 1 Configuration

The Jason-2 space segment configuration is specifically designed to guarantee the correct functioning of the spacecraft and accomplish all the mission's scientific requirements. In this report, the reverse sizing is completed along with the architecture description.

## 1.1 Vehicle shape and appendages distribution

The vehicle shape design was correlated to the structural characteristics of the multi-purpose platform PROTEUS. The platform primary structure features a truss framework, allowing for independent panel removal and easy integration.[42] The Jason-2 satellite features a modular structure consisting of a platform module, which provides vital services to the payloads, and a payload module. The overall size of the satellite is of  $1 \times 1 \times 3.7$  meters, with the PROTEUS platform occupying a cubic shape of approximately 1 meter per side.[68] All equipment units are housed on four lateral panels.[42] The mechanical interfaces between the payload and the module and between the module and the platform are established through four titanium alloy pods fastened to the four upper corners of the payload module and the platform, respectively.[84, 100] To achieve a simple and externally accessible mating, an M8 bolted connection was chosen, enabling assembly and disassembly without opening the platform or payload [100]. The payload volume is located above the platform pods and is constrained by the solar array's rotation around Y-axis, as it can be appreciated in Figure 23. Additionally, the payload must not shadow the SA and the platform thermal radiators. The payload module has the same cubic structure as the platform, with no central structure. The panels forming the cube provide structural strength as well as a surface for equipment accommodation. The lateral panels also serve as heat rejection surfaces for the thermal control of the module.[100] The S/C appendages include solar arrays and the AMR Reflector Structure Assembly. Solar arrays are mounted on deployable surfaces and were thermally isolated from the S/C body to limit thermal fluxes. The AMR includes a large reflector located on the -X face, along with a structure assembly that is positioned to face Nadir.

## 1.2 Launch configuration

The "packed" configuration of OSTM/Jason-2 was designed considering the available Delta II 7320-10 dynamic envelope.[68] The interface with the Delta II launch vehicle is through the 3715 aluminum skin and stinger adapter. The adapter is clamped to the bottom of the Jason-2 structure (-X face[106]) with a V-block type assembly, secured with two instrumented studs. The separation is triggered with an electrical command that releases the V-band clamp and the relative separation velocity is given by the action of four separation spring actuators.[105]

In order to size the stowed configuration for the satellite, the solar arrays were folded and the volume of this configuration was computed. The volume is  $3.7 m^3$ , which fits in the free volume of the fairing. The fairing's available volume was computed from the datasheet by approximating it as the combination of a cylinder and a cone (Figure 24), leading to  $28.66 m^3$ . The ring adapter's height (0.493 m) was subtracted from the available height.[105] Thus the sizing proved that the overall volume fits in the launcher envelope. However, the AMR represents an exception since its volume has to be added to the overall packaging, because it is not foldable due to the Reflector Structure Assembly.[17] This will not lead to any issues in the packaging as the total available height of the envelope is 4.897 m (5.390 - 0.493 m). In addition, aside from the main platform, the solar panels and the AMR, the other external elements did not impact the "packed" configuration. It can be appreciated that the antennae are not folded as they lack a gimbal mechanism. This is not critical due to the fact that they are engulfed in the satellite's packed volume. The same reasoning is followed for most of the payloads, as their position is not rearranged in this configuration. It can be hypothesized that this choice was made to avoid further mechanisms or any additional complexity and to ensure the correct functioning of all the payloads at the end of the Launch Phase. Moreover, the free space inside the adapter allowed for convenient storage of the 4 thrusters, which are also mounted on the -X face. Lastly, the mounted STR on the -Z face[2] is encompassed in the overall stowed configuration. In addition, the requirement on the acceptable static unbalance limit was enforced. Thus the satellite was mounted to have its centre of mass within a distance of  $d < 0.03m$  from the launcher longitudinal axis, being Jason-2 a three-axis stabilized spacecraft, with a mass at launch less than 4500 kg.[54]

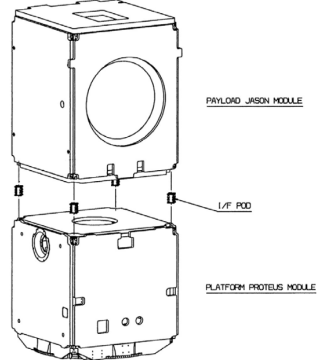


Figure 23: Modular structure. In flight configuration, the payload volume is located above the platform pods and is constrained by the solar array's rotation around Y-axis, as it can be appreciated in Figure 23. Additionally, the payload must not shadow the SA and the platform thermal radiators. The payload module has the same cubic structure as the platform, with no central structure. The panels forming the cube provide structural strength as well as a surface for equipment accommodation. The lateral panels also serve as heat rejection surfaces for the thermal control of the module.[100]

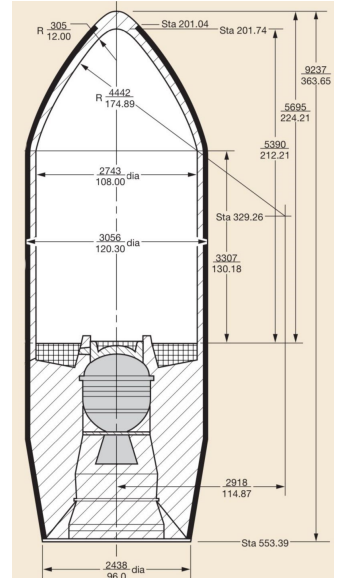


Figure 24: Payload fairing. Figure 24 shows the technical cross-sectional diagram of the Jason-2 payload fairing, detailing its dimensions and internal structure. The fairing is designed to fit the available volume of the Delta II 7320-10 dynamic envelope, with specific dimensions for the adapter and payload sections.

## 1.3 External Configuration

### 1.3.1 Propulsion System

As part of the propulsion system, Jason-2 uses a combination of 4 thrusters to perform orbital manoeuvres. These are installed under the lower plate of the -X face, opposite the tank and the remaining propulsion equipment. This configuration allows to fit both the tanks and the pipelines to feed the thrusters.[65]

*Reverse sizing:* In order to correct a possible misalignment of the centre of mass with respect to the thrust, a minimum number of three thrusters is required. The fourth thruster was added for redundancy reasons, making it possible to maintain a correctly aligned thrust even if one of the others fails. Since the attitude control is not achieved through the thrusters, they are all aligned with the direction of motion.[68]

### 1.3.2 AOCS

For attitude determination, two Star Trackers (STR) are mounted on the opposite side of the Nadir-pointing surface.[100] They are located inside a single enclosure (STA), whose position complies with two requirements: the thermoelastics effects between STA interface plane and payload interface plane shall be lower than 64 arcsec, and biases between STA interface plane and payload interface plane shall be lower than 32 arcsec. [100] The coarse sun sensors consist of 8 solar cells (4 on the pitch axis and 4 on the yaw axis).

*Reverse sizing:* The facing of the STR protects their optics and allows them to face into deep space for optimal data acquisition, exploiting the full capacity of the 22°x18° field of view. Having two STR guarantees a cold redundancy. The coarse sun sensor configuration shall provide a 4-pi steradian coverage in a non-redundant configuration.[92] Their position is due to the need for unobstructed FOV from the deployed solar arrays.

### 1.3.3 Thermal

Three radiators with silvered second surface mirrors (SSM) are placed on the honeycomb structure of the lateral panels, facing deep space. All external surfaces are covered by MLI, except for the ones requiring a field of view with Sun or Earth that are essential for the success of the mission.[106]

*Reverse sizing:* The radiator configuration allows dissipating excess heat via radiative heat transfer to the outer space. The MLI shall be placed in a way to protect the satellite from the environment but at the same time not obstruct the sensors or antennae.

### 1.3.4 EPS

Two solar array wings are symmetrically accommodated on both sides of the platform. They are deployed and structurally linked to the  $\pm Y$  sides of the satellite. When fully deployed, the solar array wingspan measures 9.7m from tip to tip. Each array consists of four 1.5x0.8m panels, making up a total area of  $9.5m^2$ . To allow the pitching of the solar arrays, two single-axis stepping motordrives are employed.[68]

*Reverse sizing:* There are two solar arrays to assure symmetry, the faces available are (-Y,+Y) or (-Z,+Z), since the satellite is perfectly symmetric, the faces selected are (-Y,+Y). The attachment on the  $\pm Y$  sides allows for a correct yaw steering approach for the panels to regulate both the power and thermal systems. Dividing each solar arrays into four panels, allows them to be folded and occupy less space.

### 1.3.5 TTMTTC

The two spiral shaped S-Band antennae for the TTMTTC system are placed on the  $\pm Z$  side of the spacecraft.[68]

*Reverse sizing:* The available faces are (+X,+Z,-Z), the antenna should be placed on the Nadir-pointing surface of the satellite which is +Z. In this way, no DOFs are added and the pointing driver of the mission can be exploited. For redundancy reasons, the other antenna should be on the opposite side such that, in the event of a safe mode, it is possible to communicate with the GS even if the Nadir-pointing condition is not satisfied. They shall also be aligned with the COG in order to have less disturbances due to their vibration.

**1.3.6 Payload** The main instrument of the Jason-2 mission is Poseidon-3: a Nadir pointing radar altimeter that has an antenna with a diameter of 1.2m placed on the +Z face. In support of this instrument, an Advanced Microwave Radiometer (AMR) is present on board; this includes a large reflector located on the +X face, along with a reflector structure assembly that allows it to face Nadir. The orbit determination system DORIS makes use of supplementary data from a precision GPS receiver (GPSP) and LRA. The DORIS-DIODE antenna is placed at the Nadir face (+Z) of the spacecraft to connect to the network of ground station. The GPSP has two omnidirectional antennae located on the top of the +X panel. The LRA is placed at the Nadir face of the satellite, this provides a reference target for the satellite laser ranging (SLR) measurements.[17]

*Reverse sizing:* Poseidon-3 and DORIS can both be placed on the same face (+Z) since they do not interfere with eachother's beamwidth. LRA must also be on this panel since it acts as a target for satellite laser ranging (SLR) measurements. AMR occupies significant space and must point at Nadir; it shall therefore be placed on the +X face, being the only one completely available. The GPSP can also fit on this face, since they do not occupy a large amount of space.

## 1.4 Internal configuration

### 1.4.1 Propulsion

The hydrazine tank is located at the centre of the platform module. The propulsion fill and drain valves are placed on the lateral panel of the structure.

*Reverse sizing:* Placing the hydrazine tank on the -X side allows for protecting the tank from possible debris impact and improves the inertia distribution.[6] The propellant mass fraction of the S/C at launch is 5%, so the CoM is not affected in a significant way by the propellant location. Additionally, being a blow-down architecture, the tank is provided with a diaphragm which prevents from undue sloshing loads, ensure consistent propellant feed minimizing centre of gravity shifts along X direction. The valves location allows for an easy access from the outside. Overall, this propulsion model is assembled as a module that can be integrated and tested as an independent unit, optimizing the platform structure.

### 1.4.2 AOCS

Regarding sensors, magnetometers and gyroscopes are mounted on the -Y and +Y faces of Jason-2, respectively. A set of three orthogonal sensors has to be implemented to determine the magnetic field vector in body frame.[23] The 3 two-axis gyroscopes are installed in an orthogonal configuration. [92]

The actuators are four reaction wheels and three magneto torquer bars. The RWs are used as primary actuators to regulate the S/C's attitude; they are in a pyramid configuration, with the tip on the X axis. The MTBs are mounted orthogonally on the +Y, +Z and -Y face.

*Reverse sizing:* The magnetometers are placed away from electronics to minimize interference with magnetic field data. This could be further reduced by placing them outside of the platform. Whilst the gyroscopes orthogonal configuration ensures redundant measurements along all three spacecraft axes.

The RWs configuration allows for each wheel to have a component of the torque along all three axes, mitigating errors due to zero-speed crossing. Moreover, a square based pyramid configuration could best suite the geometry of the PROTEUS platform which has an nearly perfect square base. Also the pyramidal configuration allows to symmetrically locate and equally space, with respect to the X axis, so that the RWs weight is balanced and torque would not be concentrated in a critical point. While MTBs configuration ensures that no unwanted magnetic field is induced in the spires, ensuring accurate torque provision.

### 1.4.3 Thermal

The internal TCS configuration must be integrated with the structural concept. The heating lines are positioned inside the platform to heat up the most critical components, which are principally the batteries, star trackers and the hydrazine tank.[2]

*Reverse sizing:* Braids and straps should be included in the subsystem to create a thermal bridge that connects internal elements with the radiators. As a parallel solution with heaters, those components are to be wrapped in MLI to decouple them from the satellite environment.

### 1.4.4 EPS

The batteries are located on the -Z face (Anti-Earth panel) and are thermally uncoupled from the rest of the platform. [2] They are MLI covered and efficiently integrated with thermal control systems to dissipate heat generated during charging and discharging cycles.

*Reverse sizing:* Due to their weight, batteries are positioned opposite to the payloads in order to have a more uniform mass distribution. To minimize the amount of wirings they could be placed under the solar panels; they could also be placed close to the DHU to minimize power losses and ensure efficient power management. [2]

### 1.4.5 OBDH

The DHU is located on the Earth panel (+Z). [2]

*Reverse sizing:* This location allows the DHU to be close to the antennae and reduce the length of the cable connections. This is also the opposite face from the batteries, which grants thermal decoupling between the two components; however, if adequate thermal protection were to be granted, they could be placed closer together to minimize power losses and ensure efficient power management. This solution implies a higher level of complexity and possible additional weight.

### 1.4.6 Payload

Following the considerations made for the external configuration of the payload, the receivers are to be placed in the internal panel of the corresponding instrument.

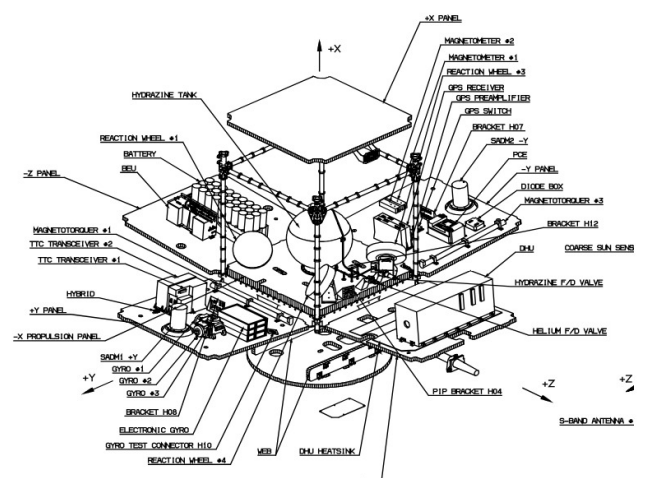


Figure 25: PROTEUS platform.

## 2 OBDH Architecture

As part of the PROTEUS family, Jason-2 relies on the multi-mission platform for the on-board data handling.[10] The primary functions of OBDH are to provide satellite mode management, failure detection and recovery, onboard visibility, payload data handling, and satellite command and control.[68]

The onboard command and data handling relies on a fully centralized system around single computer, the Data Handling Unit (DHU). The heart of this subsystem is the central computer processor MA 31750, which executes the satellite software used by the DHU for most of its tasks.

With 128 16-bit Kword of non-volatile memory, 256 Kword of random access memory (RAM) and three gigabits of dynamic RAM (DRAM) solid state mass memory, the subsystem runs OSTM/Jason 2's flight software and controls the spacecraft through interface electronics.[68] This memory is accessible via the processor from an external redundant MIL-STD-1553 B bus.[68, 44] The principal interfaces between the DHU and the platform Proteus are shown in Figure 26:

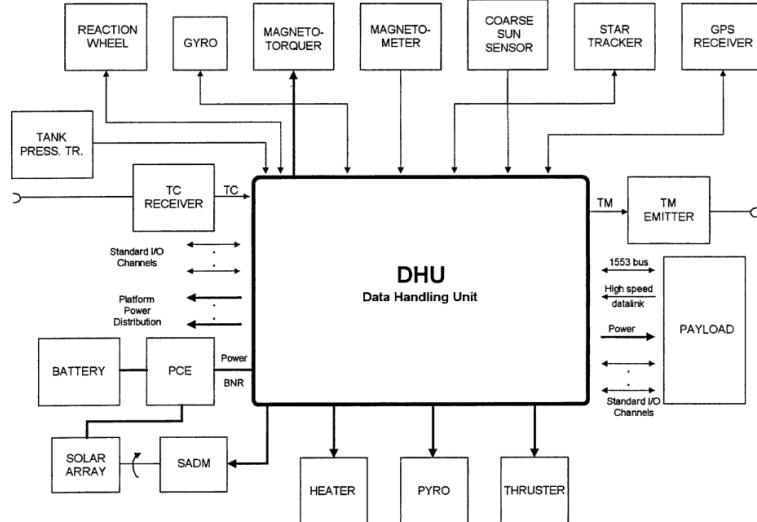


Figure 26: Proteus DHU interfaces.[44]

### 2.1 Payload data

Each payload instrument in Jason-2 has its own processor to temporarily store the collected data; an example of this is the ERC32 processor in DORIS.[17, 10] Nevertheless, the DHU still handles all the payload data transmitted to Earth each time it is in visibility of a ground station.[68] Since the beginning of the Jason-2 mission, more than 99.8% of all the raw engineering data have been acquired onboard, downloaded to the earth terminals and archived in the mission centers.[112]

The Geophysical Data Records (GDRs), provided by the on-board instruments, can be divided into three families, distinguished by increasing latency and accuracy. These families are Operational GDR (OGDR), interim GDR (IGDR) and the final GDR, and their products are identical except for the differences regarding auxiliary data used in processing shown in Figure 27.

Auxiliary Data	Impacted Parameter	OGDR	IGDR	GDR
Orbit	Satellite altitude, Doppler correction, ...	DORIS Navigator	Preliminary (MOE using DORIS data)	Precise (POE using DORIS and/or Laser and/or GPS data)
Meteo Fields	Dry/wet tropospheric corrections, U/V wind vector, Surface pressure, Inverted barometer correction, ...	Predicted	Restituted	
Pole Location	Pole tide height	Predicted	Restituted	
Mog2D	HF ocean dealiasing correction	Not available	Preliminary	Precise
GIM	Ionosphere correction	Not available		Available
Radiometer antenna temperatures coeff.	Wet tropospheric correction, Sigma0 rain attenuation, ...		Preliminary	Precise (accounting for radiometer calibration)

Figure 27: Differences between Auxiliary Data for O/I/GDR products. [10]

In terms of on-board data handling, the most challenging data set is the OGDR, since it is the most demanding in terms of latency requirements and the others are a result of in-ground processing and validation.[17] These near real time products have to be delivered to the final users within 3 hours for 75% of the time, and within 5 hours 95% of the time.[112] The OGDR data is organized into files ("segments") and stored in the

on-board mass memory provided by the DHU.[10] More specifically, the internal solid state mass memory is occupied since it allows for quick read/write operations, making it suitable for handling the large volumes of data generated by satellite instruments. At the EOL, the payload storage capacity is of 2Gbits + Housekeeping.[81] Thanks to the earth terminals configuration, the memory is downloaded every 2 hours, except for 3 “blind” orbits every 10 days, which represent less than 3% of the cases.[112]

## 2.2 OBDH processor

All of the spacecraft’s computing functions are performed by the data handling unit. The centre of this subsystem is a computer processor known as Dynex Semiconductor MA31750 high performance microprocessor, which runs the satellite software. The DHU performs most of its tasks through the central MA31750 processor: it is responsible for the power distribution to all satellite units and supports the management of the communication links. [100, 68] In Figure 28 the system configuration is shown: the DHU is based on a cold redundancy concept made up of two processor modules: the nominal one (PM A) and the redundant one (PM B). As in the case of the heaters, the nominal ones are controlled by DHU/PM A (nominal processor module) whilst the redundant ones are controlled by DHU/PM B (redundant processor module).

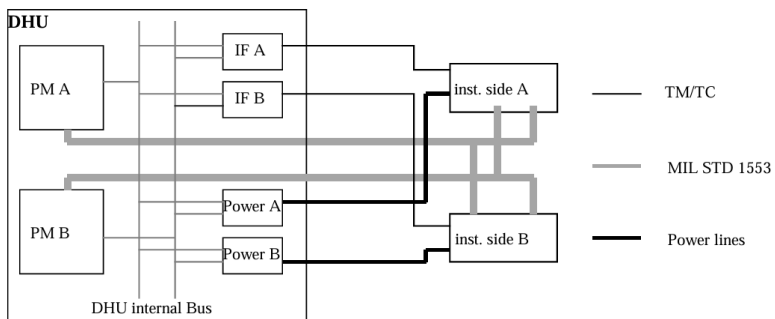


Figure 28: System configuration with redundant units and cross-strapping.[100]

The spacecraft central processor generates a clock reference, manages spacecraft data storage and ensures telemetry frame decoding. A maximum of 1,000 time-executable commands may be uplinked and stored in any given orbit pass, although many more may be uplinked. [100] Two key features of this processor have a significant impact on system performance: a 32-bit shift network and a 24-bit parallel multiplier. These sub-systems allow the processor to perform multi-bit shifts, multiplications, divisions and normalisations in a fraction of the clock cycles required on machines not having such resources. [59]

## 2.3 OBDH adopted bus

MIL-STD-1553 defines three types of bus users, called terminals: Bus Controller (BC), Remote Terminal (RT) and Bus Monitor (BM). [103] The BC acts as the master: it initiates all the transactions and it monitors the data bus and the traffic on the bus. The RTs, commanded by the BC, provide the interface between 1553 bus and the relevant sub-systems. The BM is the terminal assigned with the task of receiving bus traffic and extracting selected information to be used at a later time.[13] In particular, in Jason-2 the DHU operates as BC and the payload instruments as RTs. [100]

The allowed communications are three: from BC to one RT, from BC to all RTs and from one RT to BC, with a fixed data rate of 1 Mbit/s. There is no RT to RT exchange. [100]

As it can be seen in Figure 29, the bus is implemented on a dual redundant architecture.

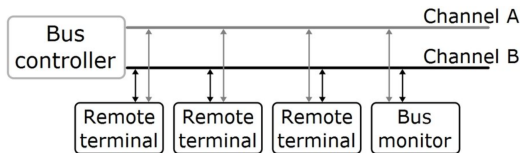


Figure 29: Dual-redundant *MIL-STD1553B* bus. [103]

In Proteus, the communication is based on an asynchronous mechanism, with an independent clock source in each payload for message transmission. In fact, the timing is highly dependent on OBSW activities such as AOCS activities, telemetry acquisition and command dispatching which are not constant along the time.[100, 13]

Payload instruments are monitored by the platform using four status: isolated, passive, stand-by and operational status. Any transition between the instrument states is allowed from ground command and after operational coordination. Only in the last one, the operational status, the 1553 bus is used for the TC/TM transit between platform and payload units.

### 3 OBDH sizing

A reverse sizing analysis was conducted to justify the choice of the OBC and memory. The procedure begins by identifying key parameters (such as code, data, TP, and frequency) and their typical values for each subsystem component. The throughput for each element is found by similarity, using their actual acquisition frequencies. Additionally, the required sizes for RAM and ROM are also calculated.

#### 3.1 On Board Computer and Memory Sizing

Sizing the OBC involves determining the number of instructions the processor must execute per second, while for the memory it requires defining the appropriate sizes for the RAM and ROM.

RAM stores both data and code, while ROM contains only code. Accurate estimation of these values requires a thorough understanding of all the spacecraft's subsystems. This involves estimating the amount of code and data each function uses, along with the instructions per second needed to perform these tasks. A function represents an action carried out by a subsystem. Figure 30 shows a representation of all functions and their respective sizing values. The values for KIPS, data, code, and typical frequency were sourced from literature.[52] As explained in section 2 each payload (P/L) is assumed to have its own processor, so they do not affect the KIPS calculation.

ADCS							
Components	Number	Code [words]	Data [words]	Typical KIPS	Typical Frequency [Hz]	Acquisition Frequency [Hz]	KIPS
Magnetometers	1	200	100	1	2		2 1
Magnetic Control	3	1000	200	1	2		2 1
Reaction Wheels Control	4	1000	300	5	2		2 5
Star Tracker	1	2000	15000	2	0,01		1 200
IMU (Gyros)	2	800	500	9	10		10 9
Coarse Sun Sensors	8	500	100	1	1		1 1
Kinematic Integration	1	2000	200	15	10		10 15
Error Determination	1	1000	100	12	10		10 12
Attitude Determination	1	15000	3500	150	10		20 300
Attitude Control	1	24000	4200	60	10		20 120
Complex Ephemeris	1	3500	2500	4	0,5		1 8
Orbit Propagation	1	13000	4000	20	1		2 40

PS							
Components	Number	Code [words]	Data [words]	Typical KIPS	Typical Frequency [Hz]	Acquisition Frequency [Hz]	KIPS
Tank	1	-	-	-	-	-	-
Thruster control	4	600	400	2,4	4	10	6
Tank Control Valve	3	800	1500	3	0,1	0,1	3
Tank Pressure Sensor	1	800	1500	3	0,1	0,1	3

TCS							
Components	Number	Code [words]	Data [words]	Typical KIPS	Typical Frequency [Hz]	Acquisition Frequency [Hz]	KIPS
Thermal Control (heaters)	1	800	1500	3	0,1	0,1	3

EPS							
Components	Number	Code [words]	Data [words]	Typical KIPS	Typical Frequency [Hz]	Acquisition Frequency [Hz]	KIPS
Solar panels	2	-	-	-	-	-	-
Batteries	1	-	-	-	-	-	-
Cable and Harness	1	-	-	-	-	-	-
Power voltage control	1	1200	500	5	1	1	5
Power current control	1	1200	500	5	1	1	5

TT&C							
Components	Number	Code [words]	Data [words]	Typical KIPS	Typical Frequency [Hz]	Acquisition Frequency [Hz]	KIPS
S-band antenna	2	-	-	-	-	-	-
Telemetry processing	1	1000	4000	7	10	20	14

System							
System	Number	Code [words]	Data [words]	Typical KIPS	Typical Frequency [Hz]	Acquisition Frequency [Hz]	KIPS
I/O Device Handlers	1	2000	700	50	5	5	50
Test and Diagnostic	1	700	400	0,5	0,1	1	5
Math utilities	1	1200	200	0,5	0,1	1	5
Executive	1	3500	2000	60	10	10	60
Run Time Kernel	1	8000	4000	60	10	10	60
Complex Autonomy	1	15000	10000	20	10	10	20
Fault Detection	1	4000	1000	15	5	5	15
Fault Correction	1	2000	10000	5	5	10	10
Kalman filter	1	8000	1000	80	0,01	0,01	80

Figure 30: Functions for every S/S.

The acquisition frequency for every function was set to at least match the typical frequency value but, where more data is required, a higher frequency was considered. In particular, the following assumptions were made:

- Star Trackers, Attitude Determination, and Attitude Control acquisition frequencies were increased given the mission's dependence on precise nadir pointing.[68] The attitude control and determination rely heavily on the star trackers: enhancing the acquisition frequency is therefore necessary to ensure that the attitude determination system can provide the required precision for the mission objectives.
- The acquisition frequency of the orbit propagation was increased due to the short orbital period of the satellite thus a high number of orbits were performed each day. This increase was considered in order to prevent errors in orbit prediction to accumulate rapidly and potentially compromise the accuracy of the spacecraft's positioning data.
- The telemetry processing acquisition frequency was increased due to the importance of constant data transmission for the mission. This subsystem is essential for maintaining continuous communication with ground control, ensuring that telemetry data is accurately downlinked with a near real-time data transmission.

In the number column, cold redundant component were not taken into account. A Kalman filter is used in the satellite which represents a significant contribution to the final results. Due to the unavailability of data for downlink and uplink, a unique value was considered for both.

To determine the required processor and memory for the analysis, all satellite's modes were evaluated. In particular, two modes were found to be the most demanding. The first mode, Communication mode, involves activating all S/S except for the PS. The second mode, Maneuvering mode, activates all the S/S except for the TTMTc.

Based on the results presented in Figure 31, it was determined that the Maneuvering mode placed the highest demand on the system. Consequently, this mode was selected for the sizing analysis for conservative reasons. A safety margin of 400% [52] was applied. This large value is justified by the assumptions made during the preliminary evaluation of the acquisition frequencies. It provides extra safety in the sizing process, ensuring contingency against potential variations in actual operating conditions.

	<b>ADCs</b>	<b>EPS</b>	<b>PS</b>	<b>TCS</b>	<b>TT&amp;C</b>	<b>OS</b>	<b>Total</b>	<b>Total Code [MB]</b>	<b>Total Data [kB]</b>	<b>Total Tp [MIPS]</b>	<b>Total Memory [MB]</b>
<b>Communication</b>	1	1	0	1	1	1				1,077	
Throughput [KIPS]	745	10	0	3	14	305	1077			5,385	
<b>Margined [KIPS]</b>	3725	50	0	15	70	1525	5385				
Code [words]	73300	2400	0	800	1000	44400	121900	0,2438			0,3818
<b>Margined [words]</b>	366500	12000	0	4000	5000	222000	609500	1,219			1,909
Data [words]	33200	1000	0	1500	4000	29300	69000		138		
<b>Margined [words]</b>	166000	5000	0	7500	20000	146500	345000		690		
<b>Maneuvering</b>	1	1	1	1	0	1					
Throughput [KIPS]	745	10	36	3	0	305	1099			1,099	
<b>Margined [KIPS]</b>	3725	50	180	15	0	1525	5495			5,495	
Code [words]	73300	2400	5600	800	0	44400	126500	0,253			0,3982
<b>Margined [words]</b>	366500	12000	28000	4000	0	222000	632500	1,265			1,991
Data [words]	33200	1000	7600	1500	0	29300	72600		145,2		
<b>Margined [words]</b>	166000	5000	38000	7500	0	146500	363000		726		

Figure 31: Reverse sizing results.

The characteristics of the processor are detailed in Table 46.

	RAM [MB]	ROM [MB]	TP [MIPS]
MA31750	0.512 [68]	0.256 [68]	3.5 [59]
Communication	1.909	1.219	5.385
Maneuvering	1.991	1.265	5.495

Table 46: Reverse Sizing results for both modes.

It is possible to observe that there is a discrepancy between the computed and the real values of RAM, ROM and TP. This can be explained by the high margin applied to the nominal computed values being a preliminary sizing. This preliminary sizing is intended to be very conservative, going on with the design more accurate information on the subsystems functions can be used to retrieve more realistic values. In fact, by looking at the non-margined values obtained in Figure 31 it can be noticed that they almost match.

## References

- [1] *1N Monopropellant Thruster, Astrium.*
- [2] Francis Arbusti and Joël Gayrard. *The Thermal Control Design and Test Philosophy of the Proteus Platform.* Tech. rep. SAE Technical Paper, 1999.
- [3] AVISO. URL: <https://www.aviso.altimetry.fr/en/missions.html?id=611&L=0>.
- [4] Y Borthomieu et al. “Calipso and Corot Lithium-Ion Battery Flight Return Experience”. In: *8th European Space Power Conference*. Vol. 661. 2008, p. 101.
- [5] C.T. Brown. *Determination of long-term compatibility of hydrazine with selected materials of construction*. United Technologies Research Center East Hartford, Connecticut, 1976.
- [6] G. Shirtliffe C. Audouy T. Guinle. “JASON-1: Orbit change to combine end-of-life safety and new science objectives”. In: (2014).
- [7] SALP CLS CNES. “Jason-2 validation and cross calibration activities”. In: (May 15, 2008).
- [8] SALP CLS CNES. “Jason-2 validation and cross calibration activities”. In: (March 24, 2022).
- [9] SALP CLS CNES. “Jason-2 validation and cross calibration activities”. In: (March 20, 2018).
- [10] CNES-EUMETSAT-JPL-NOAA/NESDIS. “OSTM/Jason-2 Products Handbook”. In: (2011).
- [11] COBHAM. *What is S-band.* URL: [https://sync.cobham.com/satcom/knowledge-library/getting-started-on-satellite-communications/what-is-s-band/#:~:text=The%20S%2Dband%20\(2%2D4GHz\)%20frequency%20is%20used,fade%20and%20other%20environmental%20interference..](https://sync.cobham.com/satcom/knowledge-library/getting-started-on-satellite-communications/what-is-s-band/#:~:text=The%20S%2Dband%20(2%2D4GHz)%20frequency%20is%20used,fade%20and%20other%20environmental%20interference..)
- [12] Rockwell Collins. *RSI 12 Momentum and Reaction Wheels 4-12 Nms with Integrated Wheel Drive Electronics.*
- [13] Data Device Corporation. *Review and Rationale of MIL-STD-1553 A and B*.
- [14] Howard D. Curtis. *Orbital Mechanics for Engineering Students (Revised 4th Edition)*.
- [15] B. Dobrotin E.P. Blackburn D. DeBra. *Spacecraft Magnetic Torques*. 1969.
- [16] Ilyas El Wafi, Mohamed Haloua, and Zouhair Guennoun. “Reaction Wheels Desaturation Using Magnetorquers Under Environmental Disturbances”. In: *2022 10th International Conference on Control, Mechatronics and Automation (ICCMA)*. IEEE. 2022, pp. 231–236.
- [17] eoPortal. URL: <https://www.eoportal.org/satellite-missions/jason-2>.
- [18] EOSOL, *Low frequency Conical Log Spiral Antenna Datasheet*.
- [19] ESA, *Space Time Explorer, Agenda, Session 8 IFP, ESTEC, 16th July 2010*.
- [20] ESA, *Concurrent Design Facility Studies, Standard Margin Philosophy Description*.
- [21] EUMETSAT. URL: <https://www.eumetsat.int/jason-2-altimetry-satellite-decommissioned>.
- [22] DD Evans and TW Price. *The status of monopropellant hydrazine technology*. Tech. rep. 1968.
- [23] J. L. Crassidis F. Landis Markley. *Fundamentals of Spacecraft Attitude Determination and Control*.
- [24] NASA Facts. “Mission OSTM, fact sheet”. In: (2019).
- [25] Navid S Fatemi et al. “Solar array trades between very high-efficiency multi-junction and Si space solar cells”. In: *Conference Record of the Twenty-Eighth IEEE Photovoltaic Specialists Conference-2000 (Cat. No. 00CH37036)*. IEEE. 2000, pp. 1083–1086.
- [26] Space Systems Forecast. *ARCHIVED REPORT Jason Series*. URL: [https://www.forecastinternational.com/archive/disp\\_pdf.cfm?DACH\\_RECNO=1341](https://www.forecastinternational.com/archive/disp_pdf.cfm?DACH_RECNO=1341).
- [27] Space System Forecast-Satellites and Spacecraft. *Jason Series*.
- [28] Jeff Foust. *Space News*. URL: <https://spacenews.com/decommissioned-earth-science-satellite-to-remain-in-orbit-for-centuries/>.
- [29] Oscar Biblarz George P. Sutton. *Rocket Propulsion Elements*. Wiley, 2016.
- [30] *GOTOFLY!: Boosting the European innovative Satellite Technologies with in Orbit Demonstration, Catalogue of IOD/IOV carriers*.
- [31] John H. Henninger. *NASA Reference Publication 1121, Solar Absorbance and Thermal Emittance of Some Common Spacecraft Thermal-Control Coatings*.
- [32] *IDS-International DORIS Service*. URL: <https://ids-doris.org/satellites/doris-satellite.html?code=JASON2>.
- [33] Zuliana Ismail and Renuganth Varatharajoo. “A study of reaction wheel configurations for a 3-axis satellite attitude control”. In: *Advances in Space Research* 45.6 (2010), pp. 750–759.

- [34] Robert R. Romanofsky James M. Budinger and Rodney L. Spence. *Direct Data Distribution from Low Earth Orbit*. Tech. rep.
- [35] “Jason 1 Launch presskit”. In: (2001).
- [36] *Jason-1(NASA-JPL/CNES) A successfull operational story throughout hardware ageing*.
- [37] “Jason-2 Project Status OSTST, Presented by Christophe Marechal, October 2019-Chicago”. In: 2019.
- [38] “Jason-2 Project Status OSTST, Presented by Christophe Marechal, October 23-27 2017”. In: 2017.
- [39] “Jason-2 Project Status OSTST, Presented by Christophe Marechal, September 2018-Azores”. In: 2018.
- [40] *Jason-3 Spacecraft and Instruments*. URL: %22https://spaceflight101.com/jason-3/jason-3-spacecraft-and-instruments/.
- [41] *Jason-3,advanced altimeter POSEIDON-3B*. URL: https://www.aviso.altimetry.fr/en/missions/current-missions/jason-3/instruments/poseidon-3b.html.
- [42] Gérard Huttin Jean-Jacques Dechezelles. *Proteus: A multimission platform for low earth orbits*. URL: https://www.sciencedirect.com/science/article/abs/pii/S1290095800800143?fr=RR-9&ref=pdf\_download&rr=88a709b2588a5237.
- [43] Kent S. Jefferies. “Analysis of Costs of Gallium Arsenide and Silicon Solar Arrays for Space Power Applications”. In: (1981).
- [44] A. Jendebay. “Proteus: data handling unit”. In: (1997).
- [45] Eric Stromswold Jim Krebs. *High Efficiency Magnetic Torquer Bars*.
- [46] NASA JPL. *NASA Spacecraft Maps Earth's Global Emissivity*. URL: https://www.jpl.nasa.gov/images/pia18833-nasa-spacecraft-maps-earths-global-emissivity.
- [47] Robert D. Karam. *Satellite Thermal Control for System Engineers*.
- [48] L.Schirone et al. “Power Bus Management Techniques for Space Missions in Low Earth Orbit”. In: (2011).
- [49] Rocket Lab. *ST-16RT2 Datasheet High-Performance Star Tracker*.
- [50] Wiley J. Larson and James R. Wertz. *Space Mission Analysis and Design (Second Edition)*.
- [51] Michèle Lavagna. *Space System Engineering and Operations - Electric Power Subsystem*.
- [52] Michèle Lavagna. *Space System Engineering and Operations - On Board Data Handling*.
- [53] Michèle Lavagna. *Space System Engineering and Operations - Thermal control system*.
- [54] Michèle Lavagna. *Space System Engineering and Operations -Exercise Session:Configuration System (CONF)*.
- [55] Michèle Roberta Lavagna. *Space System Engineering and Operations - Preliminary sizing & margins philosophy*.
- [56] Michèle Roberta Lavagna. *Space System Engineering and Operations Attitude orbit determination & Control*.
- [57] GranStal Solutions Ltd. *GS-SFA-311A-Fiber Optic Gyroscope*.
- [58] Stephen C. Ringler Luke A. Rinard Erin L. Chapman. *Reaction Wheel Supplier Survey*.
- [59] *MA31750*. URL: https://www.digchip.com/datasheets/parts/datasheet/135/MA31750.php.
- [60] Filippo Maggi. *Liquid Rocket Engine Technology (2022-2023)*.
- [61] Filippo Maggi. *Monopropellants (2023-2024)*.
- [62] Fang H. Mao X Du X. “Precise attitude determination strategy for spacecraft based on information fusion of attitude sensors: Gyros/GPS/Star-sensor”. In: *International Journal of Aeronautical and Space Sciences. The Korean Society for Aeronautical & Space Sciences* (2013). URL: http://dx.doi.org/10.5139/IJASS.2013.14.1.91.
- [63] José Meseguer, Isabel Pérez-Grande, and Angel Sanz-Andrés. *Spacecraft thermal control*. Elsevier, 2012.
- [64] Heather Monaghan. *What is the Deep Space Network?* URL: https://www.nasa.gov/directorates/somd/space-communications-navigation-program/what-is-the-deep-space-network/.
- [65] “Monopropellant Propulsion System Activities In Alcatel Space”. In: ().
- [66] NASA. *Near Earth Network (NEN) Users' Guide*.
- [67] NASA. “OSTM Newsletter”. In: www.nasa.gov np 2008 05 070 ksc (2008).
- [68] NASA. “Press kit 2008, Ocean Surface Topography Mission, Jason 2 Launch”. In: (2008).
- [69] *NASA JPL's HORIZONS*. URL: https://ssd.jpl.nasa.gov/horizons/.

- [70] *NASA Space Vehicle Design Criteria (Environment), Earth Albedo and Emitted Radiation.*
- [71] *NASA Technical Standard,NASA-STD-5001B.*
- [72] *NASA,OSTM.* URL: <https://sealevel.jpl.nasa.gov/missions/ostm-jason-2/spacecraft-and-instruments/>.
- [73] NOAA. *Space Weather.* URL: <https://www.ncei.noaa.gov/products/space-weather>.
- [74] *Orbital Propulsion Centre, Arianne Group.* URL: <https://www.space-propulsion.com/spacecraft-propulsion/hydrazine-thrusters/1n-hydrazine-thruster.html>.
- [75] “OSTM/Jason2 Mission Overview OSTST meeting-Nice, Presented by G.Zaouche,November 10 2008”. In: 2008.
- [76] “OSTM/Jason2 Mission Overview OSTST meeting-Reston, Presented by T.Guinle, October 2015”. In: 2015.
- [77] “OSTM/Jason2 Mission Overview OSTST meeting-San Diego, Presented by T.Guinle, October 19 2011”. In: 2011.
- [78] “OSTM/Jason2 Mission Overview OSTST meeting-Seattle, Presented by G.Zaouche,June 22 2009”. In: 2009.
- [79] “OSTM/Jason2 Mission Status OSTST meeting-Hobart, Presented by G.Zaouche,March 12 2007”. In: 2007.
- [80] John Stark Peter Fortescue Graham Swinerd. *Spacecraft Systems Engineering*.
- [81] Francis Douillet Philippe Landiech. *Proteus platform and application satellites*.
- [82] “Practical Horizon Plane for LEO satellite ground stations, Shkelzen Cakaj, Michael Fischer, Arpad L. Scholtz”. In: (June 1,2007).
- [83] *Proteus.* URL: <http://www.astronautix.com/p/proteus.html>.
- [84] “Proteus Satellite Structural Concept”. In: (2005).
- [85] Gragam D. Quartly. “Jason-1/Jason-2 Metocean Comparisons and Monitoring”. In: (2010).
- [86] Battin R. *”An Introduction to the Mathematics and Methods of Astrodynamics, Revised Edition”*. 1999.
- [87] Rafael. “Rafael Space Propulsion”. In: (2021).
- [88] *Rechargeable lithium battery*. 2008.
- [89] *Rechargeable lithium battery VES 100 - High Specific Energy, SAFT.* URL: <https://www.yumpu.com/en/document/view/7937750/rechargeable-lithium-battery-ves-100-high-specific-energy-saft>.
- [90] *Recurring Service Modules For Future Science Missions, A Preliminary Review*.
- [91] Lucas Reino Diez. “preliminary design of an attitude determination module for small spacecraft in leo”. In: (2023).
- [92] Michel Sghedoni et al. “Attitude and orbit control system for multimission spacecraft platform”. In: *Spacecraft Guidance, Navigation and Control Systems, Proceedings of the 3rd ESA International Conference held 26-29 November, 1996 at ESTEC, Noordwijk, the Netherlands. Edited by Brigitte Kaldeich-Schuermann. ESA SP-381, European Space Agency, 1997.*, p. 133. Vol. 381. 1997, p. 133.
- [93] *Silicon K4702 Solar Cells.* URL: <https://www.spectrolab.com/DataSheets/K4702/k4702.pdf>.
- [94] AAC clyde space. *Three Axis Magnetometer MAG-3*.
- [95] *Space Time Explorer.* URL: [https://sci.esa.int/documents/33341/36047/1567258171629-CDF\\_Space-Time\\_Explorer.pdf](https://sci.esa.int/documents/33341/36047/1567258171629-CDF_Space-Time_Explorer.pdf).
- [96] *Spiral Antenna Design with Matlab, Marcos Fioravante Buccella Espinoza*.
- [97] Walid J. Bannoura, Angelo Wade, Dwaraka N. Srinivas. *NOAA Ocean Surface Topography Mission Jason-2 Project Overview*. Tech. rep.
- [98] Nicholas L. Johnson, Eugene G. Stansbery. “The new NASA orbital debris mitigation procedural requirements and standards”. In: *Acta Astronautica* (2010).
- [99] Tensor tech. *Datasheet for Coarse Sun Sensor: CSS-10 and CSS-10S*.
- [100] *Téléchargement Manuel Utilisateur PROTEUS*.
- [101] *Téléchargement Manuel Utilisateur PROTEUS, Chapter 1*.
- [102] *Téléchargement Manuel Utilisateur PROTEUS, Chapter 9*.
- [103] *The history and basics of the Milbus 1553b.* URL: [https://www.esa.int/Enabling\\_Support/Space\\_Engineering\\_Technology/Onboard\\_Computers\\_and\\_Data\\_Handling/Mil-STD-1553](https://www.esa.int/Enabling_Support/Space_Engineering_Technology/Onboard_Computers_and_Data_Handling/Mil-STD-1553).

- [104] *U.S. Standard Atmosphere*. 1976.
- [105] ULA. "Delta II Payload Planners Guide ". 2006.
- [106] Marc Valentini and Patrick Arfi. *Proteus Small-Sat Family: Multi-Mission Thermal Control Design and Performances*. Tech. rep. SAE Technical Paper, 2006.
- [107] Rosaria Verduci et al. "Solar energy in space applications: review and technology perspectives". In: *Advanced Energy Materials* 12.29 (2022), p. 2200125.
- [108] Dwaraka Nath Srinivas Walid J. Bannoura Angelo Wade. *NASA Ocean Surface Topography Mission Jason-2 Project Overview*.
- [109] *Wallops Command and Data Acquisition Station*. URL: <https://www.ospo.noaa.gov/Operations/WCDAS/>.
- [110] James R. Wertz, David F. Everett, and Jeffrey J. Puschell. *Space Mission Engineering: The New SMAD*.
- [111] JJ.Digoin P. Tastet J.Massot Y. Borthomieu D. Prévot. "CALIPSO AND COROT LITHIUM-ION BATTERY FLIGHT RETURN EXPERIENCE". In: (2008).
- [112] G Zaouche et al. "OSTM/Jason-2: Assessment of the system performances (ocean surface topography mission: OSTM)". In: *Marine Geodesy* 33.S1 (2010), pp. 26–52.
- [113] Julian Zeithöfner. "Nominal and observation-based attitude realization for precise orbit determination of the Jason satellites". In: (2019).
- [114] Julian Zeithöfner et al. "Estimation of station-dependent LRA correction parameters for the TOPEX/Poseidon mission". In: *EGU General Assembly Conference Abstracts*. 2021, EGU21–12361.